The Earthquake Dissipative Engine: Energy Budget and Partition

S. Nielsen

Workshop on the *Mechanics of the Earthquake Cycle*

ICTP Trieste

Oct. 2023

Abstract

The earthquake cycle can be represented as an engine with fuel (elastic strain energy), dissipative processes (friction, rupture, anelastic strain) and –when the process is at non-equilibrium– a net production of kinetic energy (waves). The energy budget is challenging because:

- energy transfer is non-local, with focussed areas of energy sinks
- strain energy is quadratic, therefore the amount of energy release (or strain energy work) depends on the absolute strain (which is challenging to measure in the Earth) and not only on the strain change (easier to measure)
- dissipative processes, or friction(s) –the plural indicating friction-like processes in the wider sense– are not completely understood under the extreme conditions of earthquake rupture

We can explore the earthquake engine in the following framework:

- triggering of dynamic rupture as an energy barrier problem –you can get started with very little fuel.
- dynamic rupture propagation as a budget: energy flow and energy sinks at the rupture tip, moderated by rupture propagation velocity (not to confuse with slip velocity)
- energy scaling with rupture linear dimension (characteristic radius or width of rupture area). Energy is force $\times$ length, there appears indeed the length of rupture in the earthquake energy formula! Stopping bigger ruptures requires proportionally larger energy sinks... How to generate them?

Here we will focus on the dissipative aspects (energy sinks) of rupture and consider how this estimate of dissipation can inform the earthquake energy balance. We will be looking at how frictions can be quantified through

- observation of friction in every day's life –how can this apply to earthquake faults?
- observations of fault geology –the magnifying lens
- seismological data –looking from too far
- laboratory experimentation –looking from too close
- modelling –implicit complexity and the limits of homogenisation

1 The engine

Slab pull, slab push

The ultimate source of energy that fuels tectonic deformation in the Earth is heat from radioactive decay within the Earth mantle (releasing a power of approximately $42 \pm 2\ 10^{12}$ Watts (J. H. Davies and D. R. Davies 2010)). The resulting temperature increase causes negative and positive gravity buoyancy that drives flow, convection and magma ascent inside the Earth, and descent of colder lithospheric plates at subduction zones.

The two main drivers of plate motion are ridge push and slab pull. It is believed that slab pull is the dominant one. The stress and deformation arising from plate motion in the Earth crust and at subduction zones allows elastic energy build-up that is, at least in part, released during earthquakes **(Fig. 1)**.

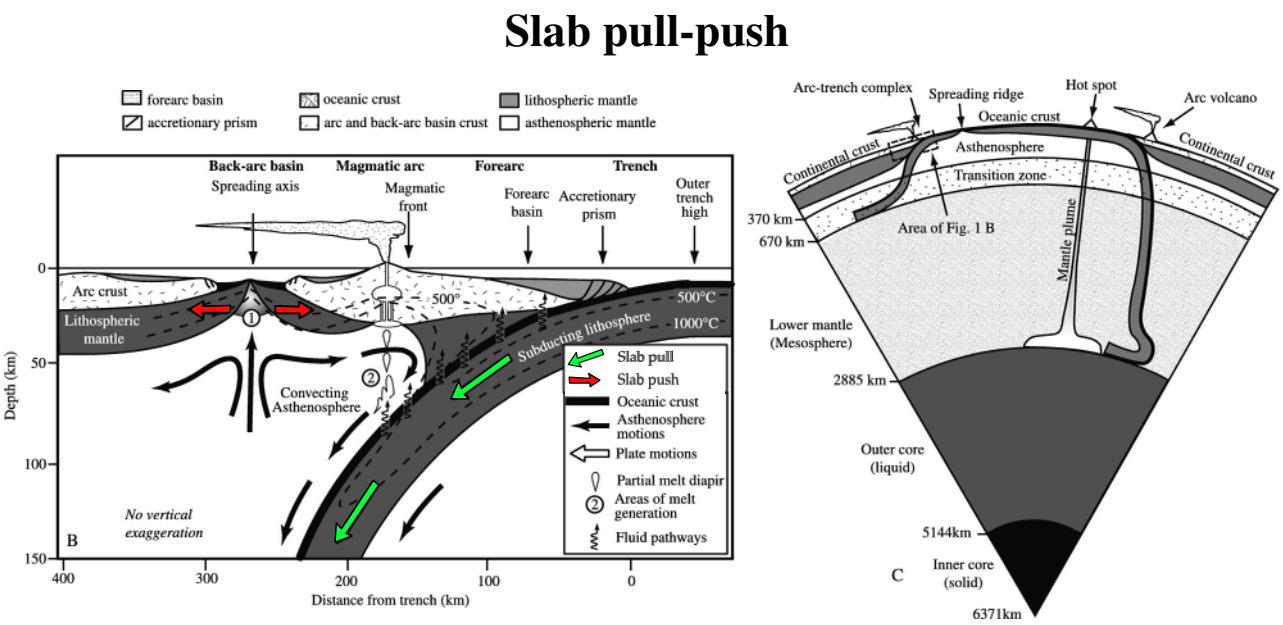

Figure 1: Schematic illustration of the oceanic plate structure, kinematics and dynamics. The main forces enabling plate motion and tectonic stress are the slab push (red arrow, expansion at the mid-oceanic ridgese, a consequence of positive buoyancy) and slab pull (negative buoyancy in the cold plunging plate). Modified from (Stern 2002).

These forces act either directly on the oceanic plates, or indirectly on the continental plate that they are in contact with. To accommodate the ensuing deformation and in response to the stress, major earthquakes take place at plate boundaries (interplate earthquakes). However, the push-pull game allows to build some amount of stress also within the plates, causing faulting and earthquakes there too (intraplate earthquakes), though in lesser magnitude and number.

For an indicative comparison with the radioactive heat power, a gross estimate[1] of average power released by earthquakes is $\approx 7\ 10^9$ Watts (i.e., a fraction of 0.017% of the energy produced by radioactive decay is released by earthquakes).

[1]The estimate can be obtained from the estimate of seismic moment ($4\ 10^{23}$ N m) released over a period of 90 years (Pacheco and Sykes 1992). The moment then needs to be converted to energy by multiplying by $0.5 10^4$ (an indicative moment to energy factor) and divided by the number of seconds in 90 years.

Exercise:

Estimate the slab pull per unit plate boundary width, due to a density contrast of 200 kg/m 3 in a slab of 70 km thickness and 500 km length. Convert the force in stress in the slab plunge direction, close to the surface.

Elastic and anelastic strain

We may define the finite shear strain (excluding rigid rotation and displacement) using the Eulerian-Almansi tensor:

$$\gamma_{zx} = \gamma_{xz} = \frac{1}{2}\left(\frac{\partial u_z}{\partial x} + \frac{\partial u_x}{\partial z} - \frac{\partial u_x}{\partial z}\frac{\partial u_x}{\partial x} - \frac{\partial u_z}{\partial z}\frac{\partial u_z}{\partial x}\right) \tag{1}$$

that uses the gradient of particle displacement (or deformation gradient) in reference to the initial (undisturbed) position. Under the assumption of infinitesimal strain, the quadratic terms can be neglected, to obtain:

$$\varepsilon_{zx} = \varepsilon_{xz} = \frac{1}{2}\left(\frac{\partial u_z}{\partial x} + \frac{\partial u_x}{\partial z}\right) \tag{2}$$

(equivalent expressions can be obtained for all 9 strain tensor elements in 3D by replacing x and z with any of x, y, z components. Because these tensors are symmetric ($\gamma_{zx} = \gamma_{xz}$) only 6 tensor elements are sufficient to characterise strain).

In most rocks, strain beyond about 2% will be accommodated by nonlinear, anelastic permanent deformation. As a consequence, to solve elastic problems (wave propagation, elastic rebound, or elastic strain energy in seismology) the assumption of infinitesimal deformation is usually made and the form (2 is used). The finite deformation arising from earthquake faulting is treated separately, often introduced in the problem as a boundary condition (or displacement discontinuity) on a surface of zero thickness (Aki and Richards 2002).

However, looking more closely at the anelastic deformation processes involved in faulting, one notes that brittle, ductile or plastic deformation and flow mechanisms are triggered in a finite volume to accommodate finite deformations. If setting out to describe the latter processes explicitly rather than implicitly, a more suitable mathematical formulation of strain would arguably be (1).

Stress and elastic strain energy

Let's first For elastic isotropic media, two elastic parameters are sufficient to relate stress σ_{ij} and strain ε_{ij}. For example, using Lame's parameter λ and shear modulus G we can write Hooke's law of elasticity as

$$\begin{gathered} \sigma_{ij} = \lambda\, \delta_{ij}\, \varepsilon_{kk} + G\, (\delta_{ik}\delta_{jl} + \delta_{il}\delta_{jk})\, \varepsilon_{kl} \\ \text{or} \\ \overline{\sigma} = \lambda\, \text{trace}(\overline{\varepsilon})\, \mathbf{I} + 2\, G\, \overline{\varepsilon} \end{gathered} \tag{3}$$

where the Kroneker δ_{ij} is such that

$$\begin{aligned} \delta_{ij} &= 0 \quad \text{if} \quad i \neq j \\ \delta_{ij} &= 1 \quad \text{if} \quad i = j \end{aligned} \tag{4}$$

and by expanding all possible individual index values we get:

$$\begin{aligned} \sigma_{xx} &= \lambda(\varepsilon_{xx} + \varepsilon_{yy} + \varepsilon_{zz}) + 2G\, \varepsilon_{xx} \\ \sigma_{yy} &= \lambda(\varepsilon_{xx} + \varepsilon_{yy} + \varepsilon_{zz}) + 2G\, \varepsilon_{yy} \\ \sigma_{zz} &= \lambda(\varepsilon_{xx} + \varepsilon_{yy} + \varepsilon_{zz}) + 2G\, \varepsilon_{zz} \\ \sigma_{xy} &= 2G\, \varepsilon_{xy}; \sigma_{xz} = 2G\, \varepsilon_{xz}; \sigma_{yz} = 2G\, \varepsilon_{yz}; \end{aligned} \tag{5}$$

Strain energy is the energy stored by a body undergoing deformation. It equates to the amount of work done by forces (or stresses) onto the body during the deformation of the body.

Take for example a case of uniaxial strain in direction x, (only $\varepsilon_{xx} \neq 0$. The stress and strain are related through Hooke's law $\sigma_{xx} = (\lambda + 2G)\ \varepsilon_{xx}$.

At each point inside a solid body (a rock for example) we can write an elementary strain energy *density* $d\rho_E$, produced by an elementary strain $d\varepsilon$:

$$d\rho_E = \sigma_{xx}(\varepsilon_{xx})\ d\varepsilon_{xx} \quad \text{work density for elementary strain } d\varepsilon_{xx} \tag{6}$$

We can obtain the energy density ρ_E resulting from a finite strain ε by integration:

$$\begin{aligned} \rho_E &= \int_0^{\varepsilon_{xx}} \sigma_{xx}(\varepsilon_{xx})\ d\varepsilon \qquad \text{energy density} \\ \rho_E &= \int_0^{\varepsilon_{xx}} (\lambda + 2\mu)\ \varepsilon_{xx}\ d\varepsilon_{xx} \\ \rho_E &= \frac{1}{2} E\ \varepsilon_{xx}^2 = \frac{1}{2}\frac{1}{E}\sigma_{xx}^2 \end{aligned} \tag{7}$$

Note that the energy density is proportional to the square of the deformation, and the square of the stress; this is important because the same amount of deformation can preduce different energies depending on the initial condition of the solid (if it is already loaded with some stress, the work will be greater).

Finally, if the solid which is under study has a volume V, to obtain the net strain energy U we need to integrate over the volume,

$$U = \int_V \rho_E(\mathbf{x})\ d\mathbf{x} \quad \text{total energy in volume } V \tag{8}$$

which in case of *homogeneous* deformation will result in:

$$U = \rho_E \times V \quad \text{if } \rho \text{ is homogeneous} \tag{9}$$

Exercise: mind experiment

A short mind experiment to explore strain energy changes. (I) A linear elastic rubber band is stretched by an unknown amount from its rest position length. (II) The same band is now stretched again, adding 2 cm to the stretching of stage (I). (III) Finally, and additional 2 cm stretching are added to stage (II). Does stretching of stage III require the same amount of work than the stretching of stage II? The elastic band stiffness is 5 N/m. Is it possible to compute the work involved in stretching stage II or stage III? Based on your conclusions, do you think that it is possible to infer the change of energy in the Earth's lithosphere, due to a deformation episode (earthquake, post-glacial rebound, dam flooding)?

Definition and strain energy change, quadratic dependence, absolute value.

Divergence theorem and work?

2 Large anelastic strain and plasticity

Anelastic deformation can be modelled, for example, by Arrhenius-type flow laws that generally depend on grain-size D and on temperature T (Pozzi, De Paola, Stefan Nielsen, et al. 2021). The shear strain-rate $\dot{\gamma}$ and the shear stress τ on a fixed plane and direction can be equated by:

$$\tau^n = C\ \dot{\gamma}\ e^{\frac{H}{RT}}\ D^b \tag{10}$$

where H is creep activation energy and C a dimensional normalisation factor. In the case of grain boundary sliding the exponents are $n = 1$ and $2 < b < 3$, with slightly increasing values if dislocation creep component is present. These laws generally fall under the behaviour of non-Newtonian viscosity, however, if $n = 1$ we can assimilate the flow to viscous shear such that $\tau = \eta\,\dot{\gamma}$ where the equivalent instantaneous viscosity is $\eta = C\,e^{\frac{H}{RT}}\,D^b$.

Anticipating on further section of this paper, we note that the shear stress τ is exponentially proportional to the inverse of temperature T. Therefore larger temperatures may allow high strain rates to be accommodated under relatively low shear stress. Because the dissipation induced by flow will increase the temperature, one can foresee that flow will promote the weakening of the solid (or fluid) where deformation occurs. Weakening in frictional slip is important in the context of earthquakes because it can promote unstable sliding and favour earthquake rupture propagation.

Exercise:

Estimate the temperature increase necessary to drop the shear stress to 10% of its initial value, assuming $\frac{H}{R} = 1950^o$ C, $T_{ini} = 250^o$C and a fixed shear rate.

A first peek into the energy budget

A very schematic representation of the elastic energy work and dissipation **(Fig. 2)** during the earthquake slip can be represented as an *average* value of work density per unit fault surface (work is in N m, the work density per unit fault surface is in Pa m^{-2} which equates to N m^{-1} or J m^{-2}). This type of graphic was introduced by Kanamori and Rivera 2006.

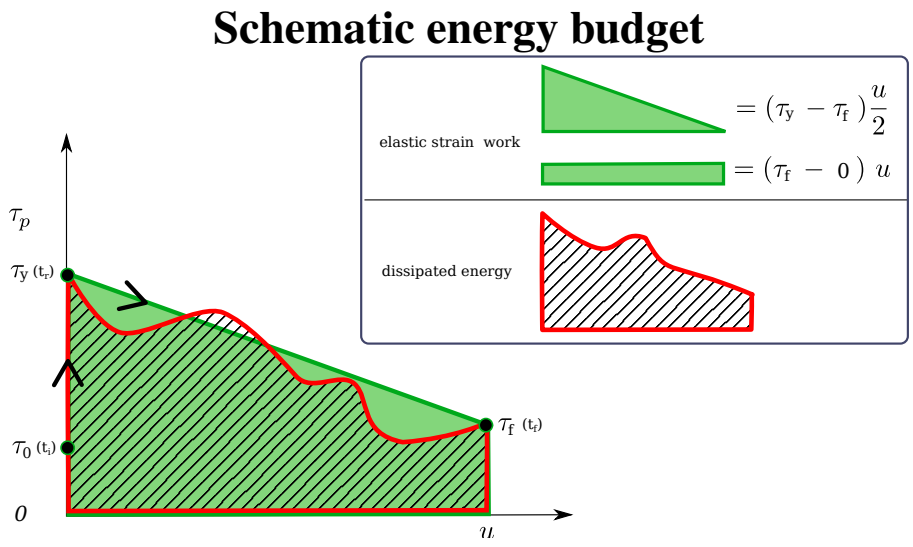

Figure 2: The work of the elastic strain energy equates to the whole green area. The dissipation is the hashed area enclosed in red curve. The dissipation area cannot exceed the elastic strain energy available (green area), or this would imply that earthquakes have a net energy creation!

Caveats of the point source picture.

3 The trigger

Irwin criterion based on energy: G is the energy released by unit crack advancement.

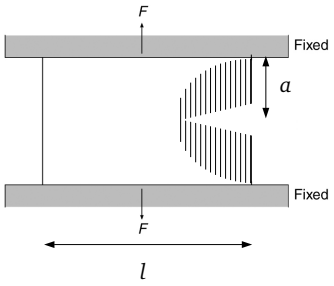

If a crack of length a appears, then elastic tension is released *roughly* in the hatched area, releasing the elastic energy(*) :

$$U = (\frac{1}{2}\sigma\ \varepsilon) \times (\pi\ a^2) = \frac{1}{2}\frac{\sigma^2}{E}\pi a^2$$

(this is per unit length in the third direction).

(*) Notice I use twice the surface of the hatched area, πa^2. The crude argument is that the free edge on the right creates a virtual "mirror" image , equating to a full disk instead of half-disk. Not a rigorous argument, but it leads to the same solution as the more complete, rigorous derivation.

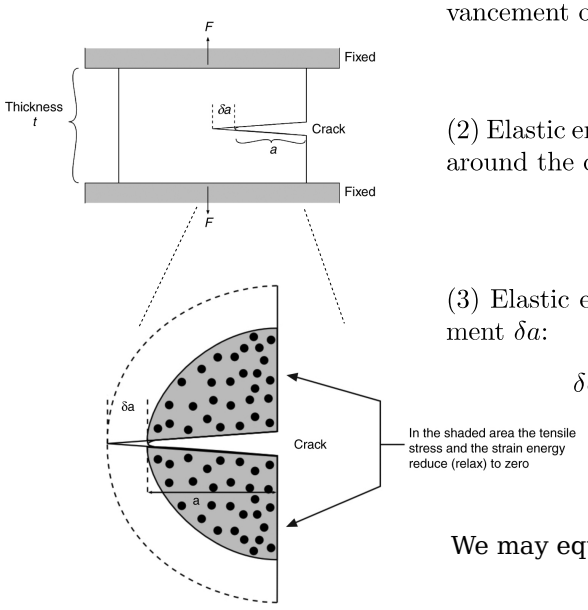

(1) Energy released by fracture advancement of δa :

$$G\ \delta a.$$

(2) Elastic energy release in the medium around the crack:

$$U = \frac{1}{2}\frac{\sigma^2}{E}\pi a^2$$

(3) Elastic energy release per advancement δa:

$$\begin{aligned}\delta U &= \delta a \times \partial_a U \\ &= \delta a\ \tfrac{\sigma^2}{E}\ \pi\ a\end{aligned}$$

We may equate (1) and (3) to get G

So that

$$\begin{aligned} G &= \pi a\frac{\sigma^2}{E} && \text{(mode I opening crack)} \\ G &= \pi L\frac{\tau^2}{\mu'}(1-\nu) && \text{(mode II shear crack)} \end{aligned} \tag{11}$$

The crack advancement dissipates energy. (For example, creation of new surface is a mechanical endothermal process, because surface energy is higher than volume energy. You may also assume that you are severing molecular bonds, therefore some work is input to separate the molecules until the bond is broken. Plastic deformation around the tip of the crack will also dissipate energy. In the case of a shear crack (although this probably was not on Irwin's mind when he designed the criterion), there is also friction, as we'll see below).

Irwin argued that the criterion for the crack advancement should be formulated as an energy budget problem. The energy dissipated should be matched by the release of elastic strain energy. Assuming that the energy dissipation per unit crack advancement G_c (critical fracture energy) in a specific material can be measured, then the criterion for crack advancement is

$$\pi L \frac{\Delta\tau^2}{\mu'} \geq G_c \tag{12}$$

Importantly we see that the energy flow increases as the square of the stress (σ here, similar to τ in case of shear crack) and also in proportion to the crack length (a here, also called L in further slides).

Note that I sneakily substituted τ with $\Delta\tau$ in the equation. $\Delta\tau$ is the stress drop, used in case of non total loss of frictional strength across a fault.

The meaning of G_c. This can be interpreted as how *blunt* ot *sharp* the crack edge is, in an analogy to a blunt or sharp knife. This is in princliple defined as a meterial property; however, what we do observe in earthquake rupture, where it is possible to estimate a seismological equivalent of G_c (Abercrombie and James R. Rice 2005), is that G_c scales with the rupture linear dimension.

An interpretation for the origin of G_c is the equivalence between crack radius of curvature and bluntness, and how they influence the stress concentration.

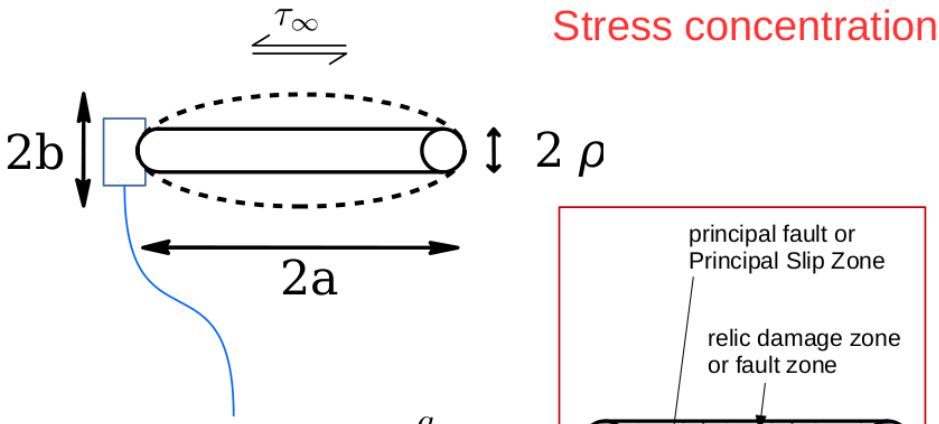

$$\tau_{max} = \tau_\infty \frac{a}{b}$$

curvature radius $\rho = b^2/a$

$$\tau_{max} = \tau_\infty \sqrt{\frac{a}{\rho}}$$

$$\tau_c = \left(\frac{\mu\, G_c}{\pi\, a}\right)^{\frac{1}{2}}$$

min. crack propagation stress

curvature radius $\rho = b^2/a$

$$\tau_{max} = \tau_\infty \sqrt{\frac{a}{\rho}}$$

assuming we start to fail, then τ_{max} is the yield strength of the rock (under shear)

equating τ_∞ and τ_c :

$$\sqrt{\frac{\mu G_c}{\pi\, a}} = \tau_{max}\sqrt{\frac{\rho}{a}}$$

$$G_c = \frac{\pi\ \rho\ \tau_{max}^2}{\mu}$$

material toughness increases with the size of the process zone

Exercise:

Consider the saw tooth model of earthquake recurrence

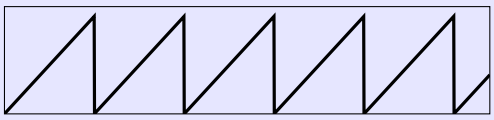

where rupture is triggered by loading up to a critical stress, and the process is repeated n times.
In light of 12, can we postulate different ways of triggering earthquake rupture?

There are indeed examples where the saw-tooth model does not seem to apply very well. This is the case for a number of intraplate earthquakes. Between 1811 and 1812 there were three large earthquakes (> 7.3) in the New Madrid Mississippi valley, in a very stable continental area with no record of tectonic strain. More recently, the 2017 M_w6.5 Botswana quake, reactivated a 2 billion year old fracture zone, with no deformation measured across the region in the previous decades.

4 Energy transfers in the earthquake process

In Appendix I the divergence theorem is used to compute the total energy change during an earthquake.

There are three main energy classes to consider in the earthquake process:

✓ built up as elastic strain and volume of elastic strain release

✓ dissipation (work done on the boundary that is the fault surface).

✓ radiation (example of instant friction release –full conversion to kinetic energy)

One can consider the earthquake problem as a transfer of energy from one class to the other. In particular, there is a convergence of elastic energy towards the propagating rupture tip, where a net energy is dissipated in the process of rupture advancement. The importance of this energy loss and how it controls the rupture process is discussed in the section below.

The energy flow

- The model of LEFM and the singularity
- What happens at the rupture tip
- Stress and energy re-distribution

In linear elastic fracture mechanics (LEFM), the solution or the stress near the crack tip is computed assuming that there region o of anelastic deformation ids infinitesimally small, therefore resulting in a non-physical stress singularity at $x = 0$. For a crack of half-length L:

$$\begin{aligned} \tau = & \frac{\Delta\tau}{\sqrt{1-\left(\frac{L}{x}\right)^2}} \\ \approx & \frac{\Delta\tau\sqrt{\pi L}}{\sqrt{2\pi r}} \end{aligned} \tag{13}$$

where τ is shear stress, $\Delta\tau$ is stress drop (or initial stress applied at infinity in case of total stress drop); x is the distance from the crack tip. A schematic graphic representation of the stress on the fault and around the rupture tip is shown in **(Fig. 3)**.

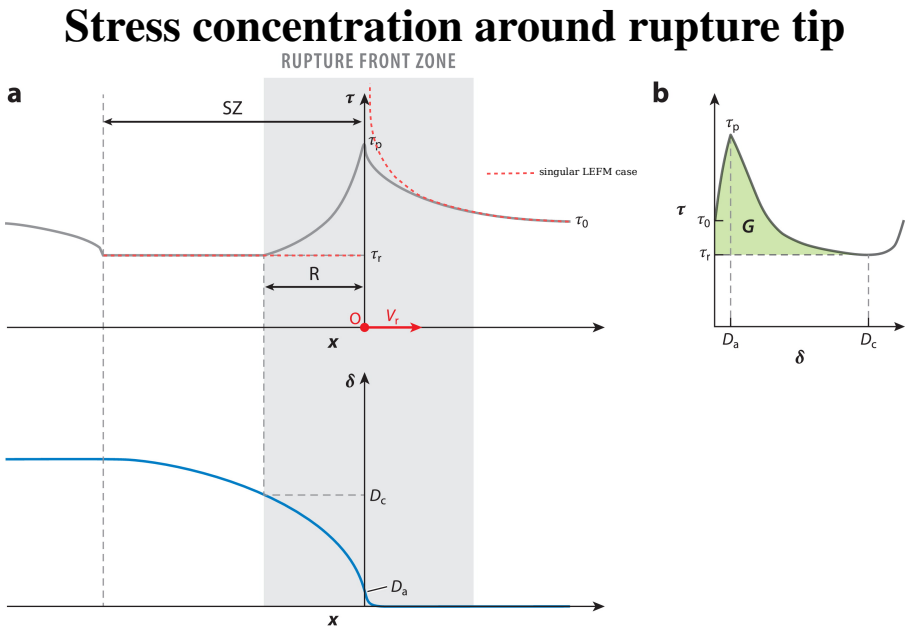

Figure 3: From Cocco, Aretusini, Cornelio, Nielsen et al. 2023

To remove the singularity, multiply (13) by $\sqrt{2\pi r}$. This results in the definition of the stress intensity. For a in-plane crack of half-length L and stress drop $\Delta\tau$:

$$K = \sqrt{\pi L}\,\Delta\tau \tag{14}$$

There is no production or loss of net energy except at the tip. This can be shown by using the divergence theorem. During a deformation, the work done against a closed surface is equal to the change of elastic strain energy inside the volume enclosed by such surface, provided that the volume behaves as a linear elastic body and that all functions are harmonic inside it. This is the case everywhere except at the crack tip, due to the singularity. When the crack advances a finite energy sink appears at the crack tip.

The energy sink can be computed mathematically by integrating the singularity, which is a tedious complex analysis exercise, with use of the residue theorem. Jim Rice introduced the J integral, on a path including the plasticity region, and showed that that the result of such integration is path-independent (a ramification of the divergence theorem).

As a result of such integration, one obtains the static energy flow (slow growing or quasi-static crack) that can be written as:

$$G_0(L) = \frac{K^2}{2\mu'}(1-\nu) \tag{15}$$

(and we can now compare this result with equation 11). The dynamic energy flow (rupture propagating at v_r that is approaching the elastic wave velocity) requires a velocity correction:

$$G = G_0\, g(v_r) \tag{16}$$

However, we can use an integral solution for a case of inhomogeneous stress drop (Fossum and Freund 1975):

$$= K(L) = \frac{\sqrt{\pi}}{2}\int_0^L \frac{\Delta\tau(x)}{\sqrt{L(t)-x}}dx \tag{17}$$

In the case of two domains with different stress drops, $\Delta\tau$ for $0 < x < L_1$ and $\Delta\tau_1$ for $L_1 < x < L$, we can integrate by parts to obtain:

$$K(L) = \Delta\tau \sqrt{\pi L} \left(1 - \left(1 - \frac{\Delta\tau_1}{\Delta\tau}\right) \sqrt{1 - \frac{L_1}{L}}\right) \tag{18}$$

noting that, if $L < L_1$ the square root becomes imaginary, and we implicitly retrieve the solution corresponding to the homogeneous case (14) (isn't maths fun!?)

Now about the case where the crack is dynamically propagating. The analytical expression for $g(v_r)$ is quite complex, in particular if we are considering the case of rupture velocity above the Rayleigh wave speed, and does not take into account waves diffracted by sudden changes in rupture velocity. It decreases homogeneously with slip velocity, gradually approaching zero for $v = c_r$. For practical purposes, ant to illustrate the concept we may use here an approximation proposed by Freund (1990):

$$g(v_r) \approx \left(1 - \frac{v_r}{c_r}\right) \left(1 - \frac{v_r}{c_s}\right)^{-1/2} \tag{19}$$

where C_r and c_s are the Rayleigh wave and shear wave velocities, respectively. We can further approximate this to:

$$g(v_r) \approx \sqrt{1 - \frac{v_r}{c_r}} \tag{20}$$

by assuming that v_r and v_s are relatively close (in most cases $0.9 < v_r < v_s$.

Then we can write an approximate balance between the available energy flow G and the critical fracture energy G_c as:

$$G_0 \sqrt{1 - \frac{v_r}{c_r}} \approx G_c$$

Recall that G_c is defined earlier as the amount of energy spent in propagating rupture of a unit length – usually considered an intrinsic property of the rock, but evidence that it is more than that and possibly a variable, with a dynamically determined value. G_c is a form of dissipation, but it does not include all the dissipation happening on a fault during rupture, only part of it, the one that affects rupture propagation and rupture velocity.

An interesting note about the situation of super-shear rupture, or more specifically intersonic rupture. Stress propagates with waves during rupture, and there are two types of body waves in a solid (plus a variety of inhomogeneous waves, including Rayleigh wave). The fastest wave is the P-wave, so causality tells us that, in principle, a rupture (almost) as fast as P-waves may propagate. It could be faster than shear-wave velocity, implying that a supersonic shock wave is generated in the S-wave field. This is observed experimentally, and, within a reasonable doubt arising from data ambiguity, also in a number of natural earthquakes. **(Fig. 4)**

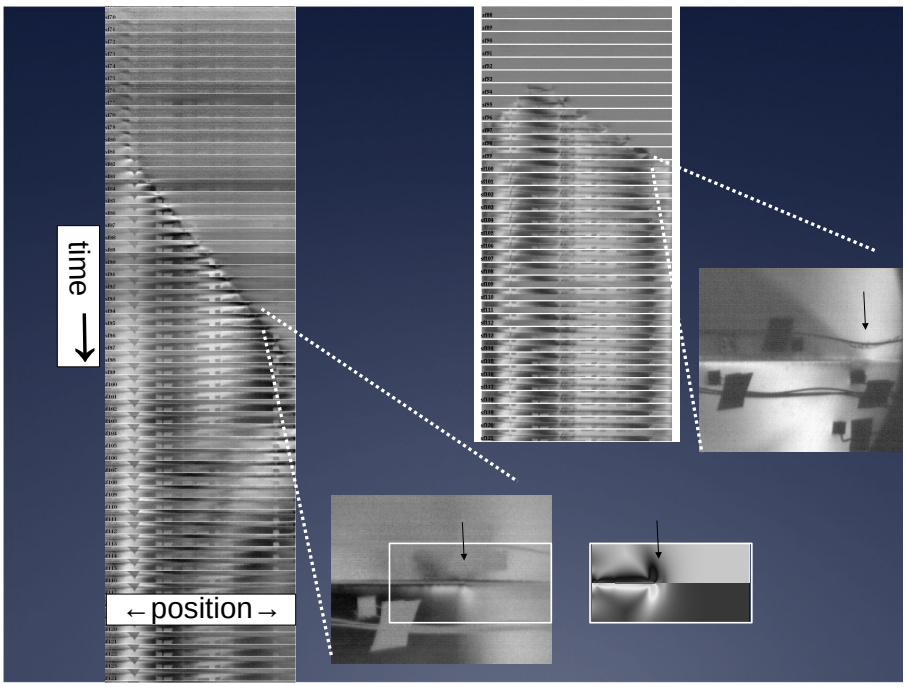

Figure 4:

There is an important possible relation between *supershear* and *off-fault damage*. The shock-wave induces an extremely fast and high strain rate, this can allow the formation of pervasive microcracks that have no time to propagate to larger lengths, and do not have time to coalesce to form bigger fractures. This behaviour has been reproduced in the lab (Doan and Gary, 2009), and proposed as an interpretation for pulverised rocks observed in the side walls of seismic faults (e.g., Arima-Takatsuki fault, Japan).

Exercise:

What processes are likely to induce the energy loss represented by G_c?

In the case of constant stress drop $\Delta\tau$ we can obtain the rupture velocity (again taking approximation 20):

$$v_r \approx c_r \sqrt{1 - \frac{G_c\,\mu'}{\Delta\tau^2\,L}\,\frac{2\,\pi}{1-\nu}} \tag{21}$$

Again, we can compare in the above expression the term in red with expressions (12) and (11). This appears to be the *ratio of critical fracture energy to the energy flow*. Therefore the same dimensionless parameter controls (1) the triggering of rupture propagation, and (2) the velocity of propagation. Note that for $G_c > L\Delta\tau^2(1-\nu)/2\pi\mu'$ the square root is imaginary which means no propagation is possible at all. In fact (21) implicitly includes the Irwin criterion.

Models that include plastic deformation, and an extended damage zone, avoid the singularity. However, the solution is compatible with LEFM, provided that the damage zone is small with respect to the crack semi-length L.

Exercise:

What happens to the rupture velocity if the crack continues to propagate under constant G_c and $\Delta\tau$? How do earthquakes stop?

Exercise:

Using the integral form of K, the energy flow, and the volume to surface conversion in the calculation of the total energy change, can you schematically map the energy transfer during crack propagation?

The direction of energy flow can be calculated in rupture propagation models; an example for 2D shear fracture (mode II) is shown in **(Fig. 5)**.

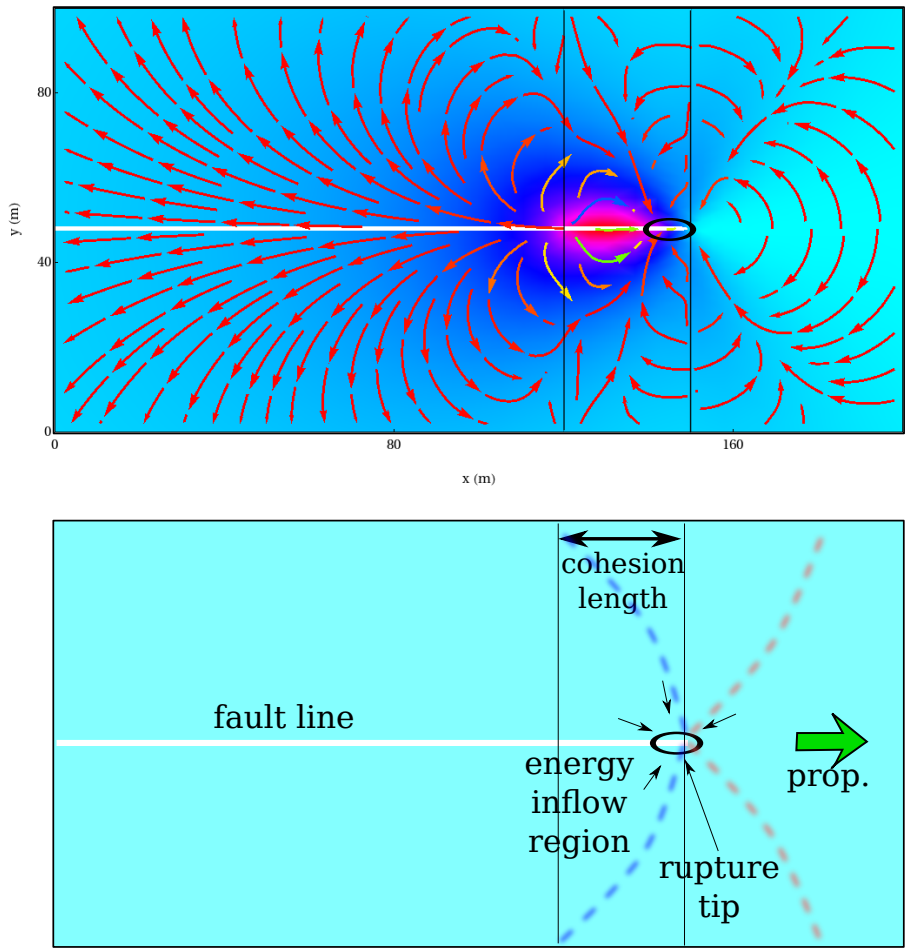

Figure 5:

Finally, a schematic visual representation of the energy redistribution during the earthquake is illustrated in **(Fig. 6)**.

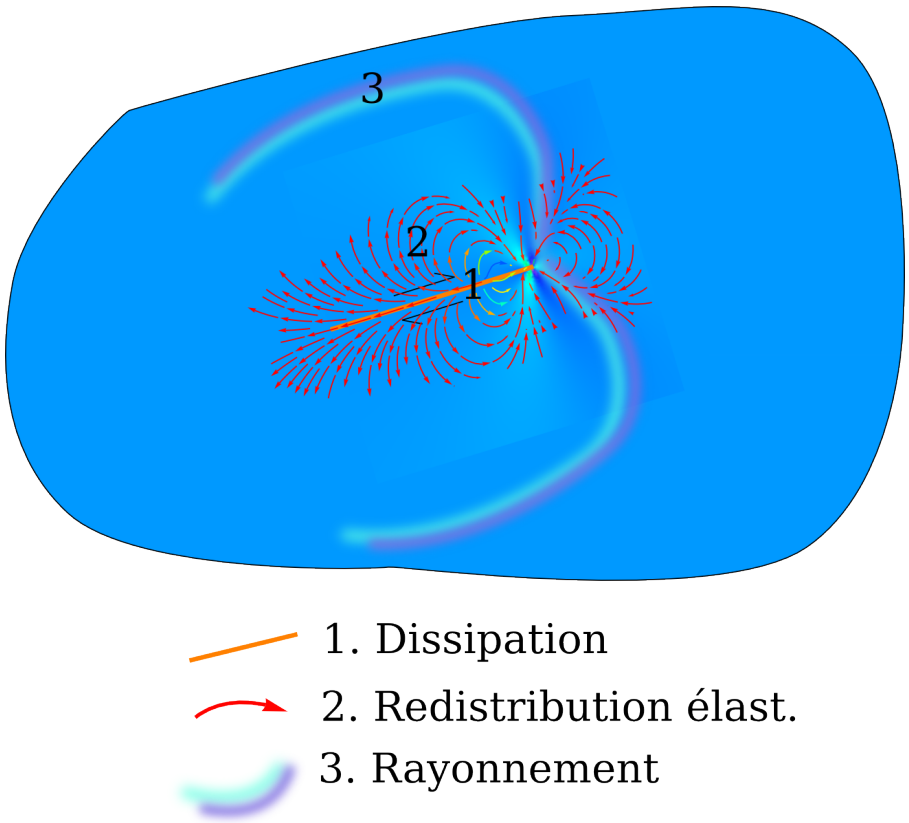

Figure 6:

5 The dissipation

This is not my fault ¯_(ツ)_/¯ : friction in every day's life

- Dry frictional contact
- Asperities
- Friction coefficient and linear normal stress dependence

It's been known since the times of Da Vinci, Amonton and Coulomb that frictional resistance to slip is proportional to normal load. A parallel can be made for rock friction as shown by Byerlee. Faults are quite different objects from every day's life engineering or household objects undergoing friction. However parallels can be made, and important concepts on friction have been cross-fertilizing between different disciplines.

A few points:

(a) The average spacing between the two rough surfaces does not vary significantly with normal load. Hertzian contact between two isolated, elastic spheres yields an interpenetration distance h varying non-linearly with the normal load in the form $h \propto F^{2/3}$. However, as shown in (Greenwood and Williamson 1966) and (Persson 2000), assuming that the surface topography of two solids in frictional contact across an area A can be mimicked by adjoining N spherical caps with average radius λ and a given probability distribution of height $\psi(z)$, the separation ω between two rough surfaces under a normal load F follows the equation:

$$\left(\frac{\omega}{\omega_0}\right)^2 = 2\log\left(N\omega_0^{3/2}\lambda^{1/2}\frac{4}{3(1-\nu_P^2)}\frac{E}{F}\right) - 5\log\left(\frac{\omega}{\omega_0}\right) \tag{22}$$

where ω_0 is the characteristic elevation of the asperities on the surface, e.g., the root mean square (rms) of the asperity height probability distribution $\psi(z)$ (z being the asperity height with respect to the reference plane $z=0$ such that $\int_A \psi(z)\,da = 0$), ν_P is the Poisson ratio and E is the Young modulus of the medium. A schematic illustration of the meaning of the ω, ω_0 and λ in the above equation is provided in **(Fig. 7)**.

Rough surfaces and fault veins: a mathematical frame

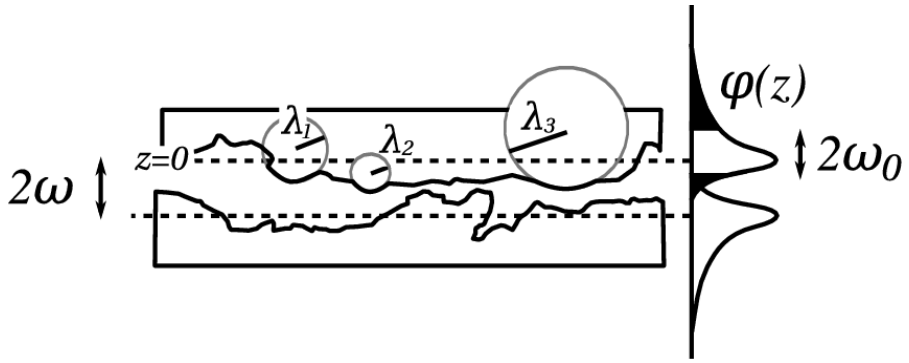

Figure 7: Illustration of ω, ω_0 and λ in the equation. $\psi(z)$ is the probability density function of the asperity heights with respect to a reference or average elevation (dotted line). Finally, ω_0 is defined as the rms of distribution $\psi(z)$ and λ as the characteristic radius in the distribution of the spherical arcs fitting individual asperities. From S. Nielsen, di Toro, and Griffith 2010

(b) The area of real contact between two rough surfaces increases proportionally to normal load. It appears that the separation ω is weakly sensitive to normal load σ_n, resulting for practical purposes in a bounded value $\omega = 2\,\omega_0 \rightarrow 3\,\omega_0$. Therefore λ can be considered as constant, and the major change upon normal load increase is than increase in the number of asperities N, but modest increase in the contact area $\pi\lambda^2$ of each individual asperity. Therefore the increase of area (and N) is proportional to the normal load.

If friction is proportional to the real area of contact, then Greenwood (Greenwood and Williamson 1966) essentially has explained Coulomb's law of friction $\tau = \mu'\,\sigma_n$.

Letting α be the proportion of real contact area vs. total area, it can be shown that $\alpha = \sigma_n/\sigma_c$; the contact asperities are under a compressive stress close to the material strength σ_c, in a state of incipient plastic yield (Dieterich and Kilgore 1996; Persson 2000).

At first glance it is counter-intuitive that in point (a) above, the separation distance between the two surfaces is a highly non linear function of normal load, while the area of contact described in point (b) shows is proportional to normal load. Indeed the behavior of a distribution of asperities is quite different from that of a single, isolated Hertzian ontact. One key mechanism is that, under an increasing normal load, the effective contact area increases principally by increasing the total number of contact asperities (rather than by increasing the area of existing asperities). These results are discussed at length in texts of tribology (study of friction, e.g. Greenwood and Williamson 1966; Persson 2000) but also to some extent in bibliography on fault mechanics (Brown and Scholz 1985).

In the case of fluid filling the voids between the two fault edges, we may slightly modify the above definition of α as a the ratio of normal to yield stress, due to the presence of the additional pressure P in the fluid, for example, in case of melt, the pressure generated by extrusion of the viscous melt, or in case of thermal pressurization, the increase in fluid pressure due to the temperature rise. We can obtain a modified relationship by simply writing the total load across the area as the sum of two contributions:

$$\sigma_n = \alpha\,\sigma_c + (1-\alpha)\,P \tag{23}$$

In presence of a pressurized fluid the real contact area will be smaller, in that

$$\alpha = \frac{\sigma_n - (1-\alpha)P}{\sigma_c} \approx \frac{\sigma_n - P}{\sigma_c} \tag{24}$$

and the friction will be reduced in proportion to the pressure P such that $\tau = \mu'(\sigma_n - P)$.

(c) The contact asperities are in a state of incipient yield stress. The initial contact across a rough surface is a very tiny fraction of the total area, therefore all the normal load is concentrated to such a level that the contact yields plastically. The number of contacts gradually increases until the load is sufficiently distributed that plastic deformation slows down, but remains close to the critical yield stress (incipient yield). In such a state the contacts age, and friction continues to increase very slowly, it is shown by experimental measurements that static friction increases with the log of time **(Fig. 8)**.

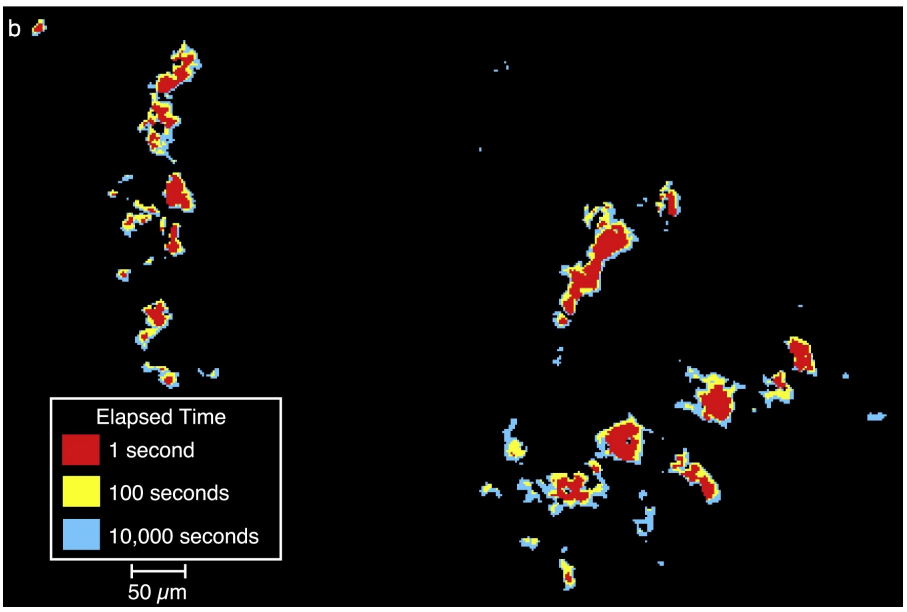

Figure 8: Example of evolution of contact asperities in time; experimental result from (Dieterich and Kilgore 1996).

(c) Sliding and abrasion. Under sliding asperity contacts will disappear and new ones will form. The average contact time will decrease with slip velocity, reducing the ageing. Contacts leave grooves on the opposite face and become smeared in the direction of slip. This process is quite visible on either experimental friction surfaces **(Fig. 9)** and on natural faults **(Fig. 10)**.

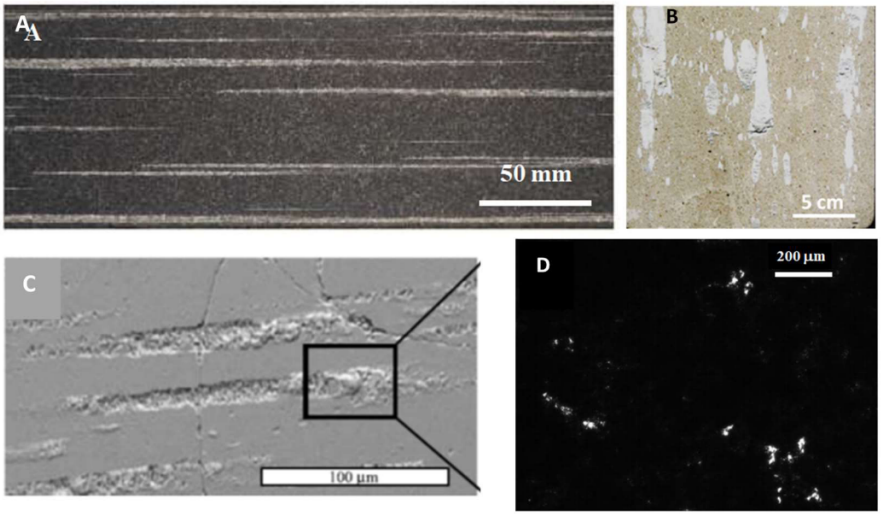

Figure 9: Fraom (Reches, Chen, and Carpenter 2019)

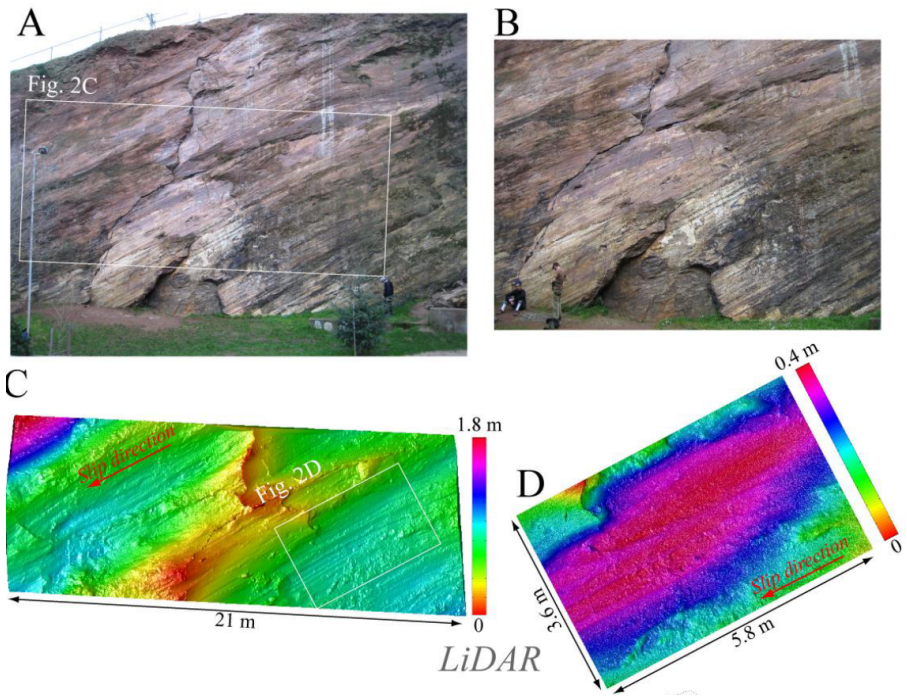

Figure 10: From (Candela, Renard, Klinger, et al. 2012)

If the sliding becomes fast, typically more than 0.1 m/s, and, in the case of seismic sliding, of the order of 1 m/s or more, the heat released by the shearing of the asperity contacts will not have much time to diffuse away from the asperity, therefore the temperature can locally rise (although the bulk temperature may still be modest). This phenomenon can induce a particular type of frictional weakening described in the *Flash weakening* section further down.

Effect of fault roughness on rupture triggering

One consequence of fault roughness and contact asperities, is that sections of the fault surface are devoid of any contacts. One may try to fit circular patches within non-contact areas surrounded by asperities, and find the circle with the maximum radius possible. As seen previously in eq. (12: $\pi L \frac{\Delta\tau^2}{\mu'} \geq G_c$), the rupture propagation criterion includes the half-length L of the initial fracture. Asperity-free areas being subject to no traction, they can be assimilated to initial fractures of radius L that re-distribute stress on the peripheral contacts. Increasing normal load will make new contacts appear and the size of the traction-free areas will shrink. **(Fig. 11)** As a consequence, a subtle balance between the nature of rugosity and the normal stress will regulate the potential for unstable rupture propagation on a fault **(Fig. 12)** **(Fig. 13)**.

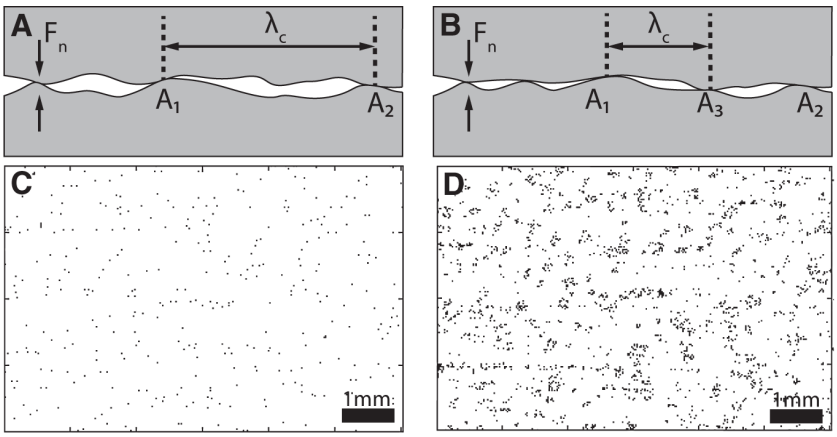

Figure 11:

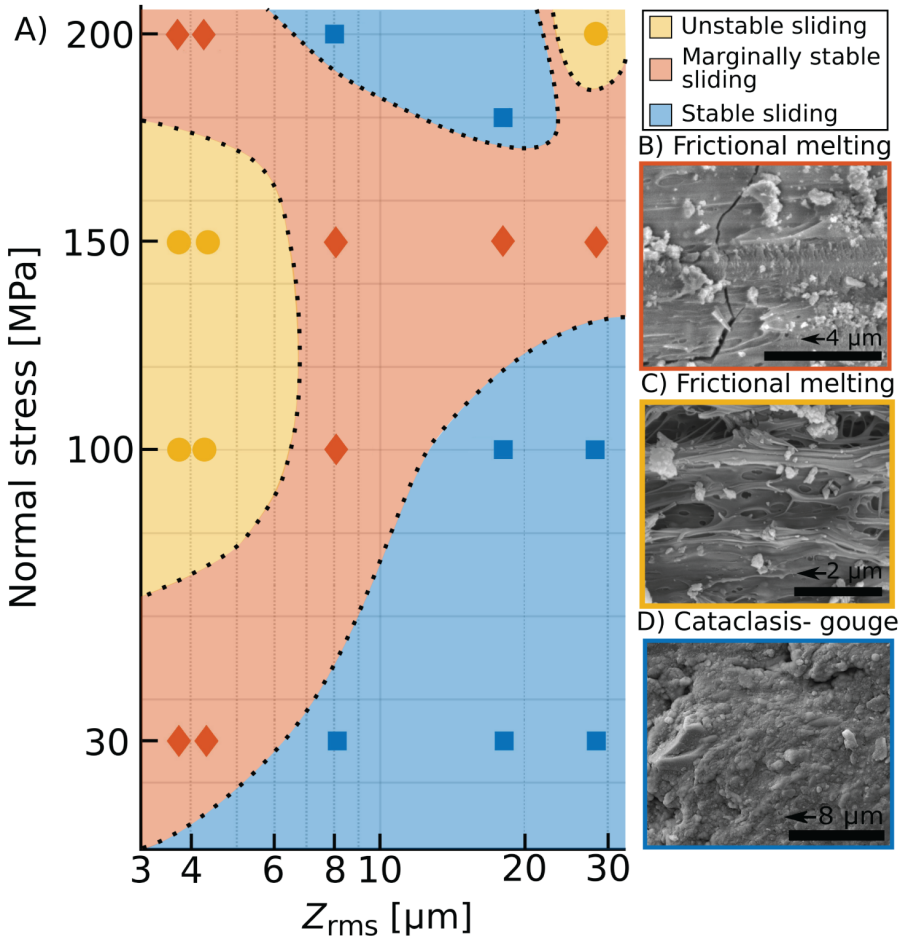

Figure 12:

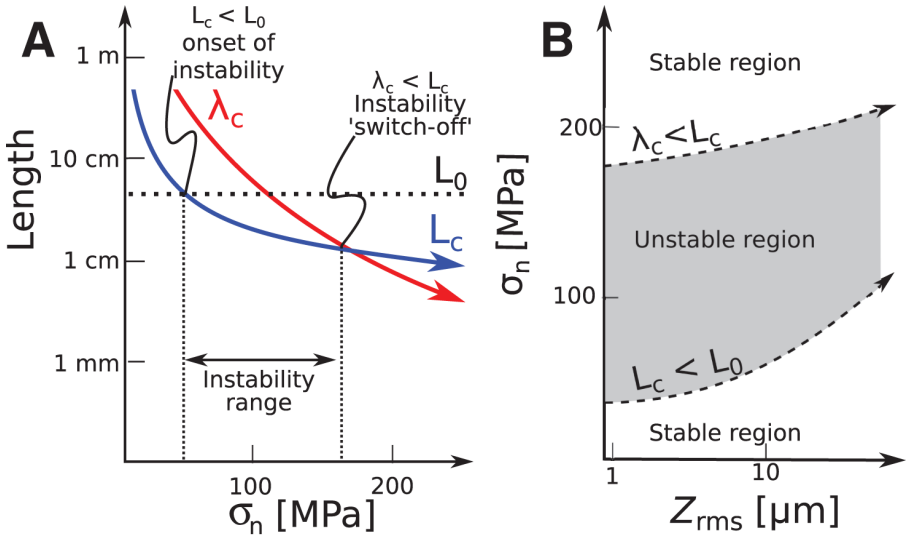

Figure 13:

Upscaling from micro to macro deformation –frictions on faults

- An infinitesimally thin surface? Major faults show a wide (up to hundreds of m) damage zone
- Fault structures in the field

  - Damage zone
  - Fault core
  - Principal Slip Zone (PSZ)
  - Pulverised rock

- Distributed region of plasticity vs LEFM
  - Equivalent models provided that the plasticity region is relatively small
- Models where dissipation in the volume around fracture tip is equated to frictional work on the fault
  - In what cases can this work?
  - Stress excess outside fault surface
  - Shear parallel to the fault
  - Thermally triggered, endothermal processes
  - Off-fault damage with no shear deformation.
  - Volume of contact asperities: friction is seldom a strictly surface process.
  - Dissipation form non-shearing processes, or from shearing that does not project onto the fault surface cannot be factored-in as friction, because there is no frictional work-to-slip proportionality
  - The friction-compatible work is only from shear that is compatible with double couple motion (strain tensor components on 2 orthogonal planes) and within a reasonably thin zone
- Reproducing faults in the lab
- Damage generated during the earthquake rupture . . . See Jean-Paul Ampero's class?. . .

(Fig. 14)

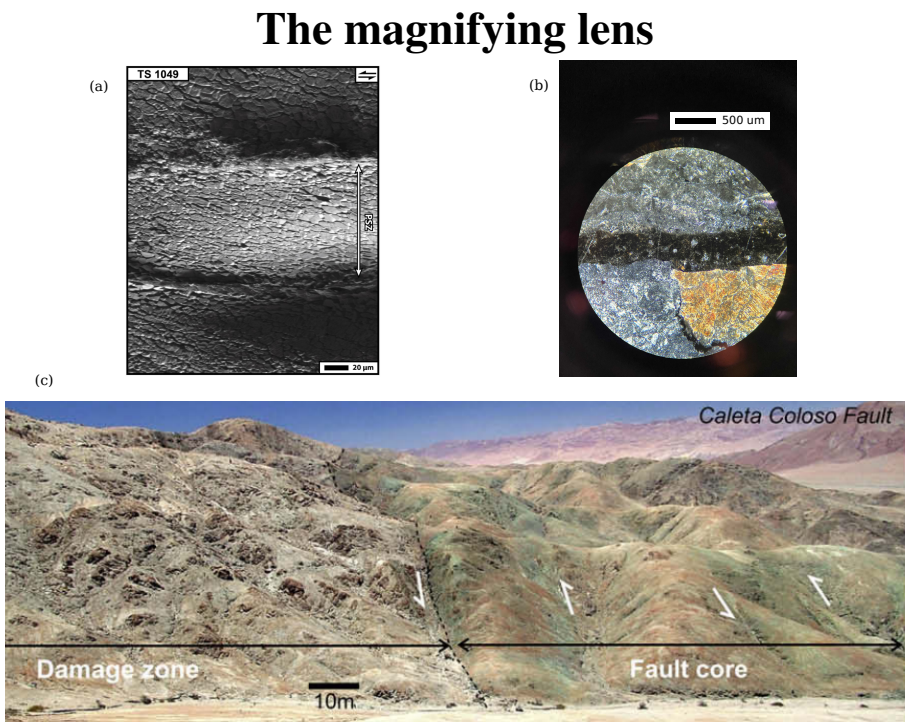

Figure 14: Faults from the microscale to the kilometer. These are a few examples among many in the lab and in the field (from (a) (Pozzi, De Paola, Stefan Nielsen, et al. 2021) (b) Nielsen (personal collection) and (c) (T. Mitchell and Faulkner 2009)). Can we assume a zero thickness plane? If so, what is the scaling linear (just a magnifying lens) or non-linear (something fundamentally different in the dimensionless ratios at large and small scale?

(Fig. 15) (Fig. 16) (Fig. 17)

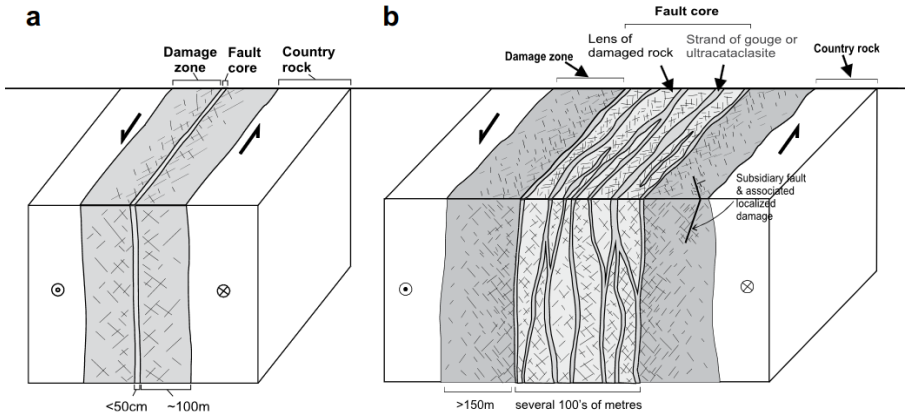

Figure 15: Form (T. Mitchell and Faulkner 2009)

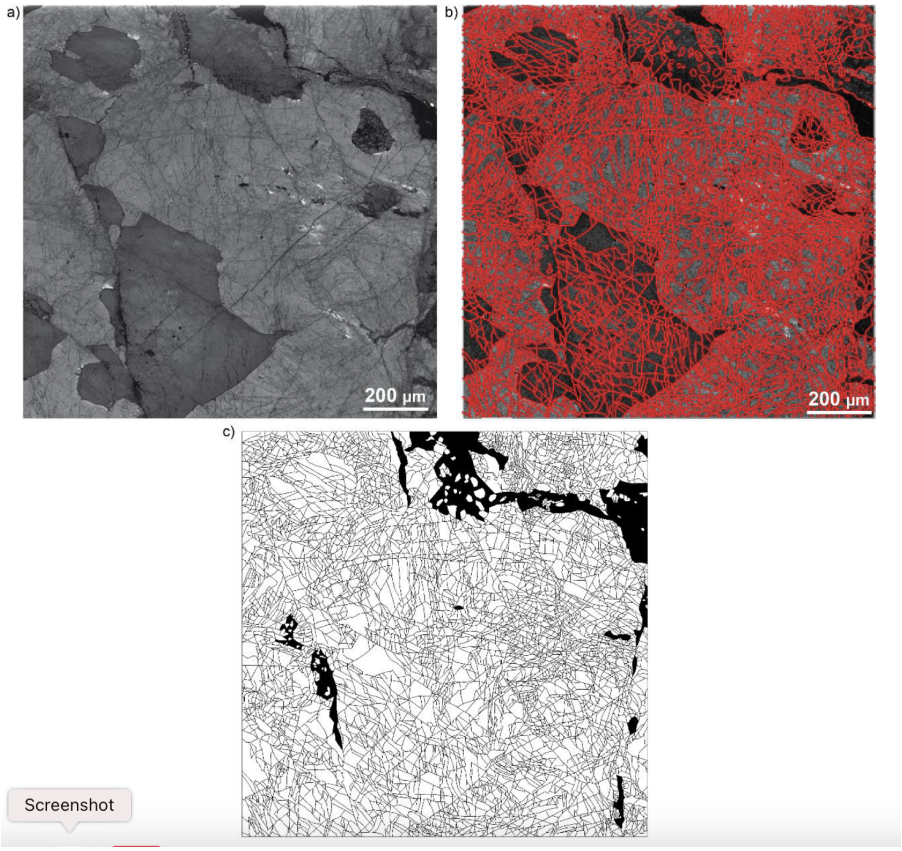

Figure 16: Form (Aldrighetti 2023)

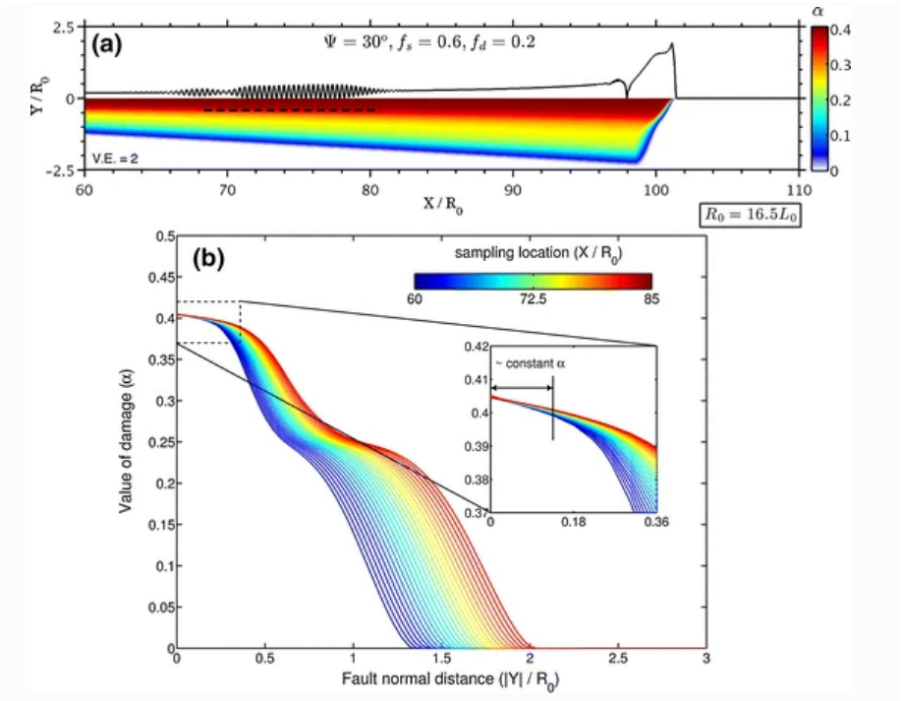

Figure 17: Form (Xu, Ben-Zion, Ampuero, et al. 2014)

(Fig. 18)
(Fig. 19)
(Fig. 20)

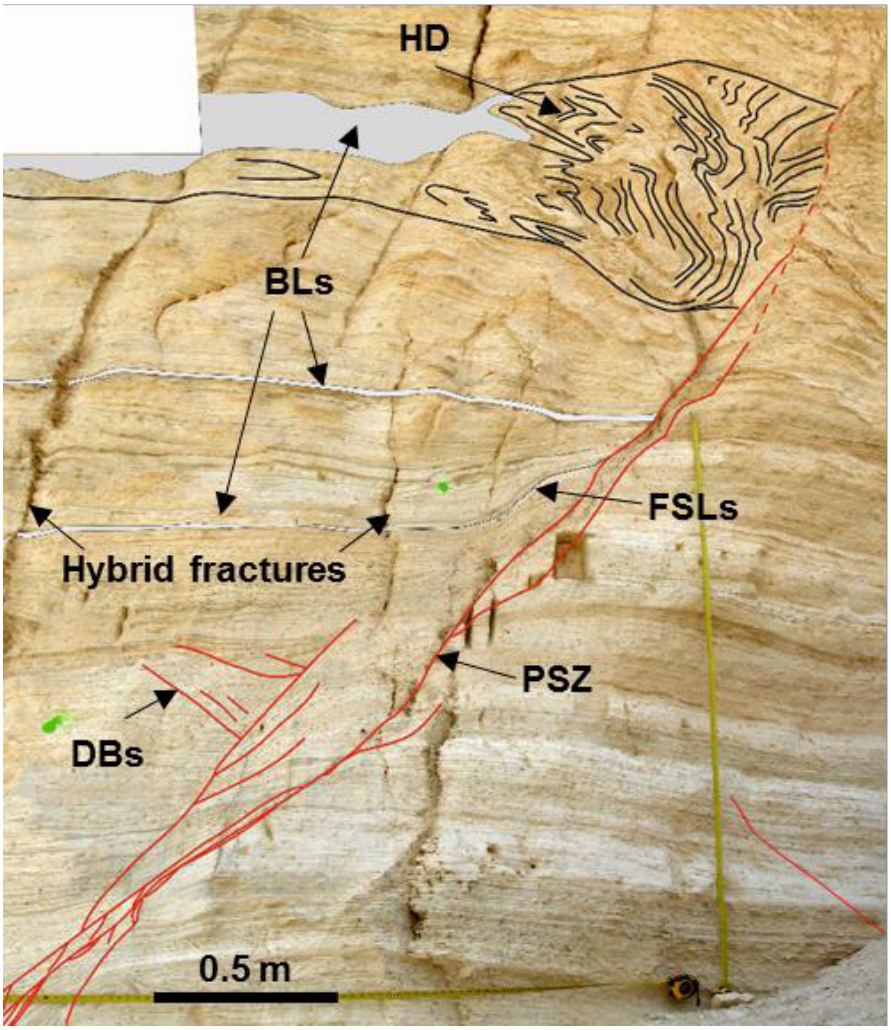

Figure 18: From Bullock et al., in prep.

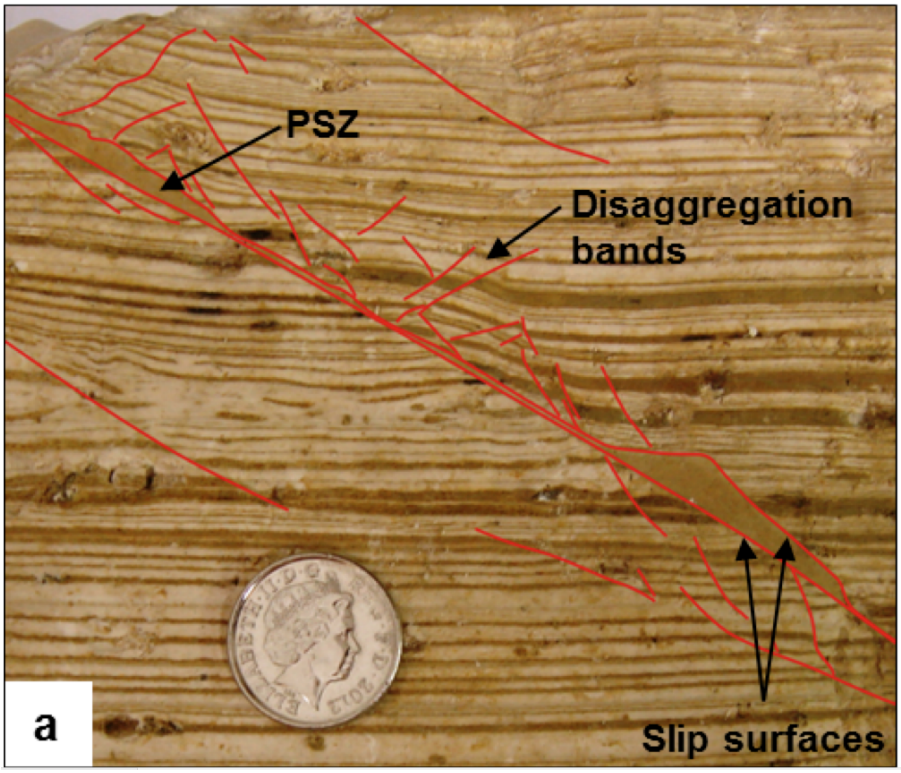

Figure 19: From Bullock et al., in prep.

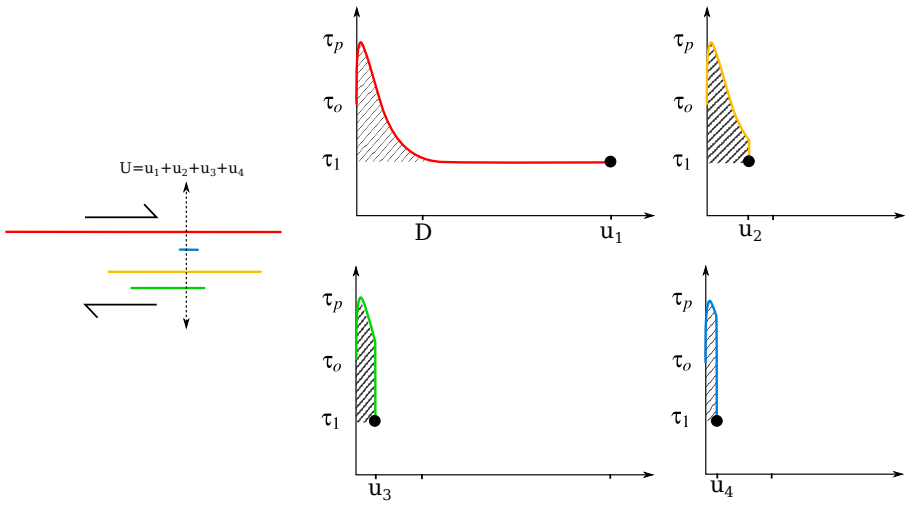

Figure 20: From Bullock et al., in prep.

Sliding friction at slow slip rates

See Allan Rubin's class!. . .

A very large body of literature exist that has explored the rate and state laws both theoretically and experimentally –Alan Rubin to gave a much more complete overview, but to recall the general

formulation, we can write:

$$\begin{aligned} \mu &= \mu_0 + a \log \frac{V}{V_0} + b \log \frac{\theta V_o}{D_c} \quad (a) \\ \frac{d\theta}{dt} &= 1 - \frac{V \theta}{D_c} \quad (b) \\ \mu_{ss} &= \mu_0 + (a-b) \log \frac{V}{V_0} \quad (c) \text{ (steady-state limit)} \end{aligned} \tag{25}$$

(Alternatives with other evolution laws for θ exist). The rate-and-state laws reproduce well experiments in the range 1-500 $\mu m/s$, and allow to simulate, among other things, the nucleation phase of earthquakes and a rich spectrum of fault behaviour from stable creep to unstable slip episodes and earthquakes.

The steady state condition allows defining a critical stiffness:

$$\begin{aligned} K_c &= \frac{\sigma_n V}{D_c} \left(\frac{d\mu_{ss}}{dV} + F(V, \theta_f) \right) \\ &= \frac{\sigma_n (b-a)}{D_c} \quad \text{(no inertia)} \end{aligned} \tag{26}$$

where σ_n is the effective stress normal to the fault and $F(V, \theta_f)$ is a generic term for inertia. When a slider bloc or, by analogy, a fault has $K < K_c$ then it can accelerate and become unstable, which might generate a slow or a fast earthquake (where the fault stiffness can be defined as $K = \mu'/L$).

At high slip velocity (typically V > 0.1 m/s) dramatic frictional weakening is observed 21 that cannot be simulated by the modest logarithmic velocity dependence of (25) **(Fig. 21)**.

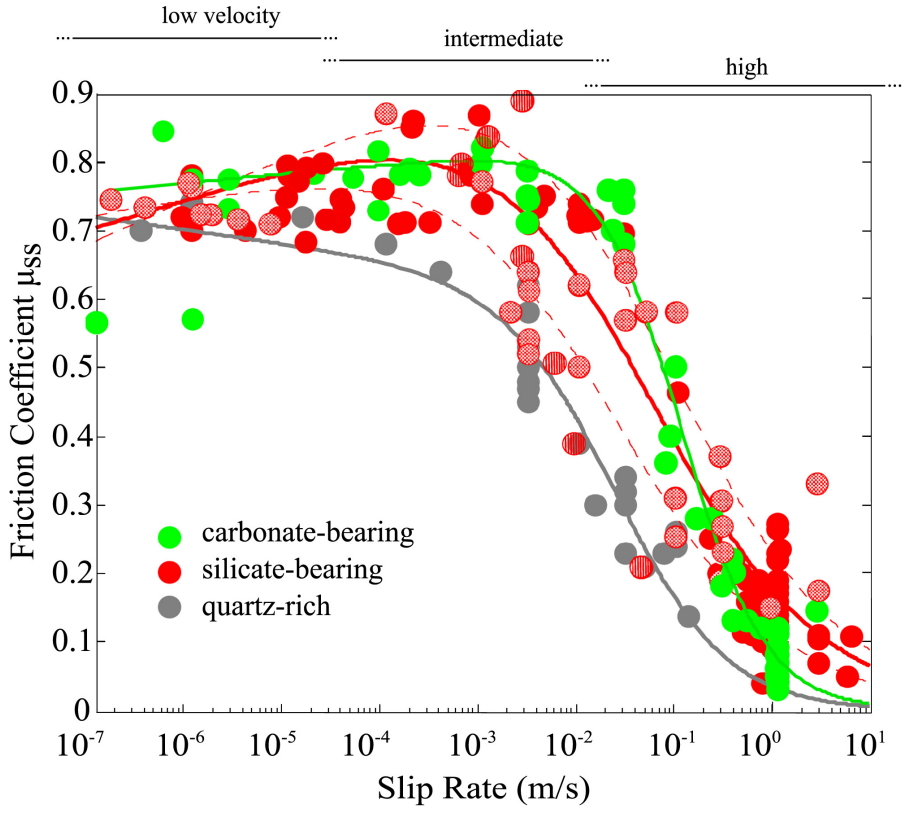

Figure 21: From (Spagnuolo, S. Nielsen, Violay, et al. 2016)

Because the velocity dependence at high slip rates in a variety of fault rock materials appears to a good approximation to behave as negative power-law of velocity, an empirical fit can be obtained by combining(25) with a velocity denominator such that:

$$\mu = \frac{\mu_0 + a \log \frac{V}{V_0} + b \log \frac{\theta V_o}{D_c}}{1 + (V/V_c)^p} \tag{27}$$

An alternative, and more general definition of critical stiffness can then be derived, that allows for instability in a wider range of parameters (Spagnuolo, S. Nielsen, Violay, et al. 2016).

Exercise:

Assuming that a fault at a plate boundary is under stable sliding at 10 mm/y (plate motion). During an earthquake there is a stress drop from 60 to 20 MPa when the fault slip accelerates. Estimate the slip velocity that would generate an equivalent friction drop during the earthquake, assuming that a rate and state friction as (25-c) is acting. Assume that the fault depth is at 3 km depth, that the rock density is $\rho = 2800$ kg m^{-3}. Use representative values of $a - b = -0.004$ for a rate-weakening rock. Repeat the estimate using 27 with $V_c = 0.05$ m/s and p=1. In which case the fault slip acceleration is more realistic?

There is a fundamental change in the frictional slip at rates above a few cm/s. The main reason is the temperature rise that takes place when high power from frictional slip produces heat at a faster rate than could be efficiently be evacuated by diffusion. In the coming section we will analyse a few processes where heating is responsible for enhanced weakening.

Sliding frictions at fast slip rates:

As roundly summed up by (Madariaga 2007), one can consider that earthquake faults are *slippery when hot*. Effectively the heat is generated by the sliding itself, and there are several ways that temperature rise can weaken the dynamic sliding friction.

The heat rate (or power) of frictional sliding under a shear stress τ and velocity V

$$q(t) = 1/2\,(\tau(t)\,V(t) - q_s(T(t)))\,, \tag{28}$$

where τ is shear stress, V is sliding velocity, and q_s rpresents thermally triggered energy sinks (e.g., latent heat, etc); q is introduced as a heat source on the fault surface, represented in the 1D thermal diffusion equation (z is the fault-perpendicular direction):

$$\partial_t T = \kappa \partial_z^2 T + \frac{\delta(z)\,q}{\rho\,c}; \tag{29}$$

finally, the temperature of the fault surface resulting from the solution of (29) will have a feedback effect on the shear stress τ, assuming that it has a thermal dependence:

$$\tau(t) = f(V,\, T,\, \ldots) \tag{30}$$

Therefore the 3 above equations are coupled in the frictional weakening problem.

Exercises:

1) The penetration depth of a diffusive process is of the order of $z = \sqrt{2\kappa t}$. Do a back-of the envelope calculation of average temperature within z for the conditions of question (1), after 0.1 s, 1 s, 2 s, 10 s. Assume a shear stress of 10 MPa, a sliding velocity of V=1 m/s and a diffusivity of $10^{-6}\mathrm{m}^2\mathrm{s}^{-1}$.
2) Compute the temperature rise vs. time on the fault surface (z=0) for the same conditions as above.
3) Compute the temperature profile perpendicular to the fault after the same time intervals as question (1).

Useful equations:

The well-known solution of the diffusion equation Carslaw and Jaeger 1990 for a heat flow Φ imposed at the border of a half-space is obtained by integrating

$$T(z,t) = \frac{1}{\rho c\sqrt{\kappa\pi}} \int_0^t \frac{\Phi(t)}{\sqrt{t'}} e^{-z^2/(4\kappa\tau)}\, dt'$$

which, for a fixed flow $\Phi = \tau V$, yields the temperature profile:

$$T(z,t) = \left(\frac{2e^{-\frac{z^2}{4t\kappa}}\sqrt{t}}{c\rho\sqrt{\pi\kappa}} - \frac{z\,\mathrm{erfc}\left(\frac{z}{2\sqrt{\kappa t}}\right)}{\kappa\rho c} \right) \frac{\tau V}{2}$$

A foreword on experimental techniques

It is challenging to conduct experiments at high velocity, and the technical breakthroughs were achieved between the eighties and the early 2000s.

(Fig. 22)
(Fig. 25)
(Fig. 24)

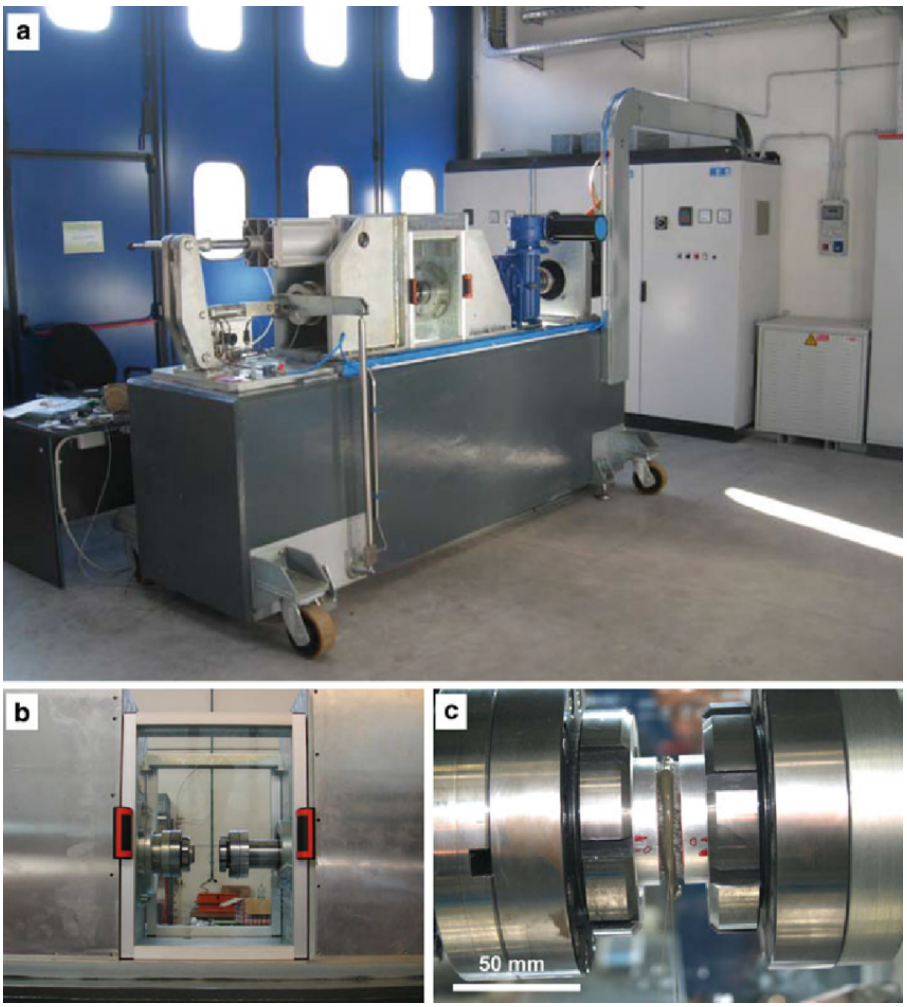

Figure 22:

Figure 23:

Figure 24: From (Pozzi, De Paola, Stefan Nielsen, et al. 2021)

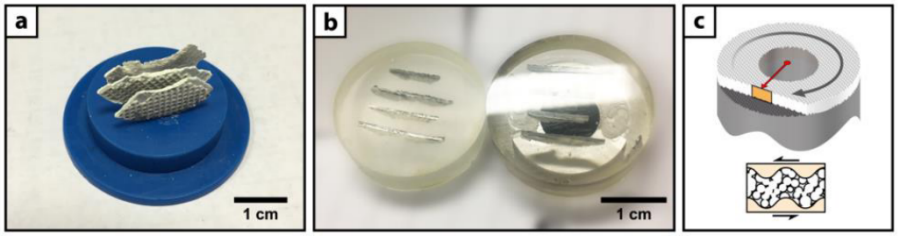

Figure 25: From (Pozzi, De Paola, Stefan Nielsen, et al. 2021)

Play **VIDEOs** showing experiments at HV

Flash weakening

Flash weakening and heating of contact asperities has been proposed as a model for high velocity friction evolution (Archard 1959; J. R. Rice 2006). There are strong experimental indications (Goldsby and Tullis 2011; Violay, Di Toro, S. Nielsen, et al. 2015) that this model is relevant for high velocity experiments, in both silicate- and carbonate- built rocks, at least in the first millimeters of slip or until melting or decomposition of the rock minerals creates an almost contiuous, amorphous interstitial layer. One motivation to explore flash heating is that weakening precedes the substantial rise of the background temperature of the sliding interface. Initial thermal weakening may be achieved only if local temperatures $T + \Delta T$ at asperity contacts are much higher than the background temperature T **(Fig. 26)**.

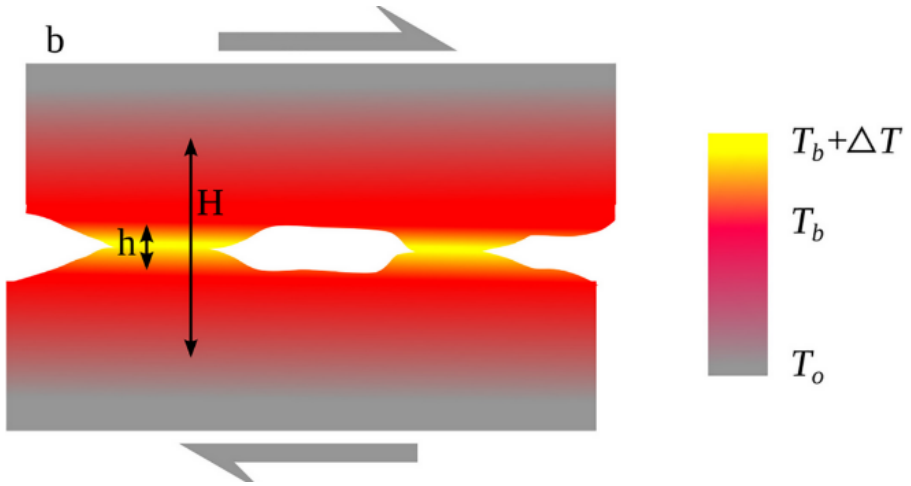

Figure 26: Local temperature rise at contact asperities can weaken friction very effectively and much earlier than the rise of bulk temperature becomes consistent. From (S. Nielsen, Spagnuolo, Violay, and G. Di Toro 2021)

The FW model considers that the lifetime of asperity of linear dimension D is indicatively $t_c = D/V$. For an asperity sheared under incipient yield stress τ_c, the heating results from frictional power $\tau_c V$. Assuming that heat diffusion is mostly perpendicular to the fault, during the asperity lifetime, with $q \approx \tau_c V = \text{const.}$ the local temperature rise is $\Delta T = \gamma \tau_c V \sqrt{t_c} = \gamma \tau_c \sqrt{V D}$, and the time during contact at which the asperity weakens is $t_w = (T_w - T)^2/(\gamma \tau_c V)^2$. Upon defining a threshold temperature $T_w = T + \Delta T$, a minimum slip rate V_w can be computed at which shear resistance is lost within the duration of an asperity contact lifetime:

$$V_w = \frac{1}{\gamma^2 \tau_c^2 D} \text{ Max}\left[T_w - T,\ 0\right]^2 \tag{31}$$

The average strength of an asperity contact during its lifetime will be $\tau_a = (\tau_r(t_c - t_w) + \tau_c t_w)/t_c$, where τ_r is the residual shear stress supported by the weakened asperity. Assuming an asperity population with dominant dimension D, using $\tau_p = \alpha \tau_c$, $\tau_w = \alpha \tau_w$, $\tau = \alpha \tau_a$ and noting that $t_w/t_c = \tau_c (T_w - T)^2/(\gamma^2 \tau_c^2 V D) = \tau_c V_w/V$ it is found (J. R. Rice 2006) that the effective sliding shear stress is:

$$\tau \approx (\tau_p - \tau_w)\left(\frac{V_w}{V}\right) + \tau_w \tag{32}$$

for $V > V_w$. We find, however, that the onset of weakening (first centimeters of slip) in the experiments is smooth and better reproduced by the regularised form:

$$\tau \approx (\tau_p - \tau_w)\left(\frac{V_w}{V + V_w}\right) + \tau_w \tag{33}$$

which can be used for all V. This may qualitatively reflect the behaviour of a distribution of asperities whose weakening is gradually triggered at different velocities depending on their size, rather than an abupt onset of weakening of all asperities at the same threshold velocity V_w.

One of the peculiarities of the model described by equations (32) is the absence of explicit dependence on normal stress. However, the evolution of background temperature T can be factored into (31), rather than using a constant V_w. Thus the effect of τV as a heat source implicitly includes normal stress, which will reflect on the temperature rise and therefore on the velocity weakening through V_w.

Indeed during the initial part of the slip $\tau = \tau_p = \mu_s \sigma_n$ where μ_s is the initial friction coefficient (of the order of 0.6 before onset of weakening). Thus, although the initial (peak) stress will be higher under higher normal stress, temperature rise and weakening will be accelerated by a similar proportion. As a consequence, the weakening slip distance and the fracture energy may not be significantly

altered by a change in normal stress. This behaviour was indeed observed in a synthesis of different high velocity friction laboratory experiments (S. Nielsen, Spagnuolo, Violay, S. Smith, et al. 2016; S. Nielsen, Spagnuolo, S. A. F. Smith, et al. 2016).

Physical models that reproduce weakening due to thermal effects can take into account different processes, such as (1) the flash weakening model for the instantaneous velocity dependence, and (2) the thermal diffusion to simulate the bulk temperature evolution, and (3) the presence of heat sinks due to phase transitions that are triggered by the temperature rise. All three effects are taken into account in (S. Nielsen, Spagnuolo, Violay, and G. Di Toro 2021) where experimental weakening curves are reproduced numerically as shown in **(Fig. 27)**.

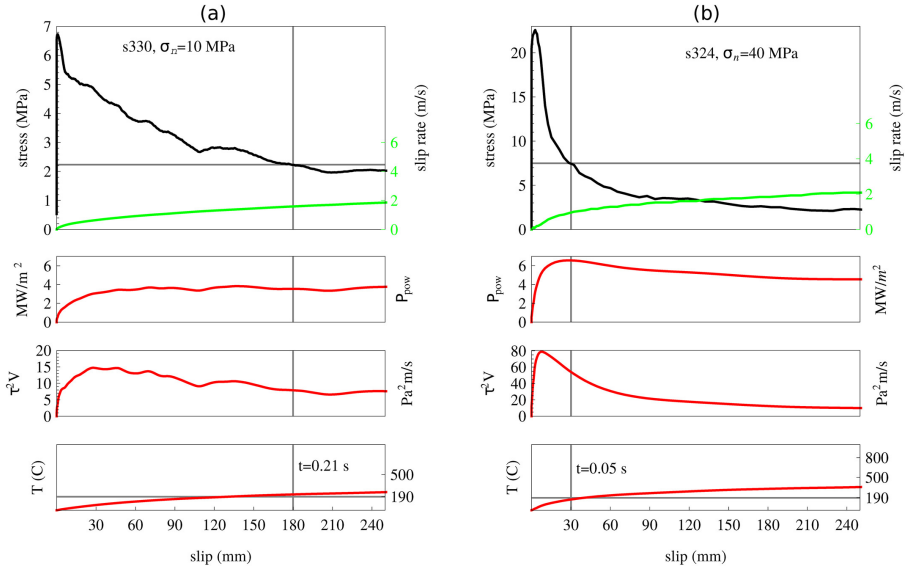

Figure 27:

Looking for a supporting argument for the role of bulk temperature in frictional weakening, and to verify the numerical model, (S. Nielsen, Spagnuolo, Violay, and G. Di Toro 2021) did two experimental test that were identical, except in one case the sample was cooled by immersion in liquid Nitrogen. The initial temperature of the sample, in the region around the frictional sliding surface, was estimated at $-140 < T_i < -50^o$C. The mechanical curves obtained from the tests **(Fig. 28)** show a delayed weakening in the case of the cooled sample **(Fig. 28)** –the weakening is reproduced reasonably well by the model by using an initial temperature $T_i = -70^o$C, which is compatible with the estimate.

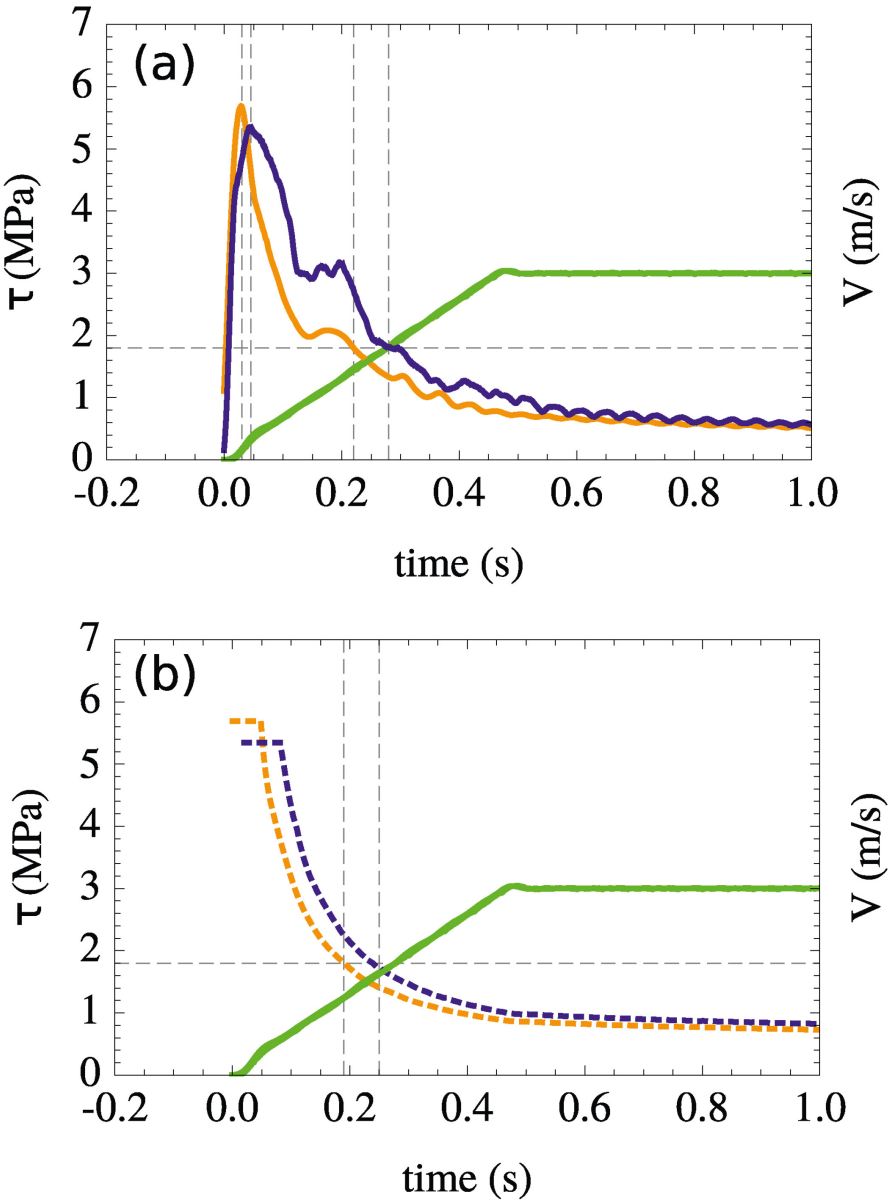

Figure 28: From (S. Nielsen, Spagnuolo, Violay, and G. Di Toro 2021)

Superplasticity

It is known that crystal plasticity, under favourable circumstances, can be described by flows laws such as (10) extrapolates to extreme conditions of shear rate. Usually experimentally measured at conditions of $\dot{\gamma} \ll 1$, but they have been verified at $\dot{\gamma} \approx 1$, a conditions known as superplasticity.

Having observed structures typically formed under a crystalline plastic flow known as grain boundary sliding (GBS), on samples of calcite sheared at seismic conditions **(Fig. ??)**, Pozzi, De Paola, Stefan Nielsen, et al. 2021 set out to verify experimentally whether flow laws could explain the extreme weakening at high speed and whether different types of rock could be behave differently.

If a flow law can indeed be extrapolated, it is likely to be governed by different, and yet unkonwn parameters than those esimated for low strain rates. However, a general signature of the thermal dependance is expected, and can be highlighted by taking the log of 10 such that

$$\log \tau = \left(\frac{H}{n\,R} \right) \frac{1}{T} + \frac{1}{n} \log \frac{\dot{\gamma}\, D^m}{C} \tag{34}$$

and noting that regardless of the values of H, n, m, C, a loglinear form should be observed such that

$$\log \tau = A\frac{1}{T} + B. \tag{35}$$

(Fig. 29)
(Fig. 30)
(Fig. 31)

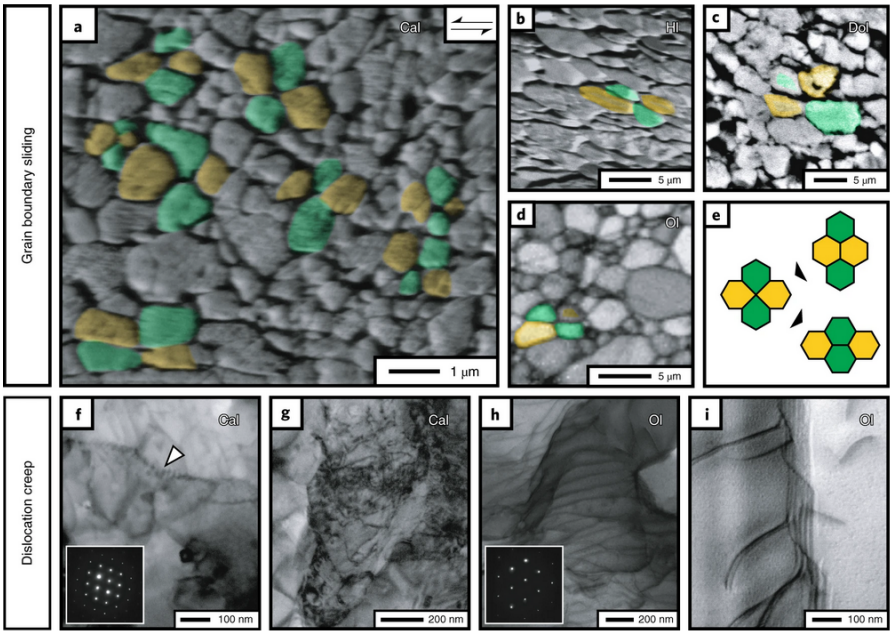

Figure 29: From (Pozzi, De Paola, Stefan Nielsen, et al. 2021)

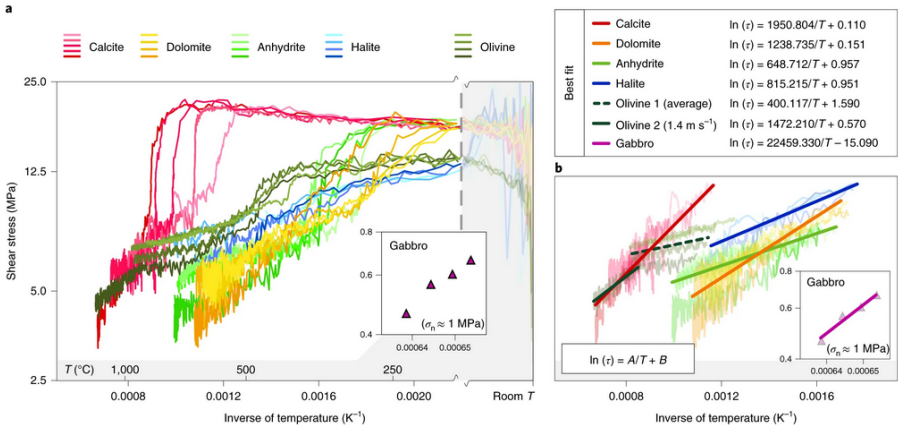

Figure 30: From (Pozzi, De Paola, Stefan Nielsen, et al. 2021)

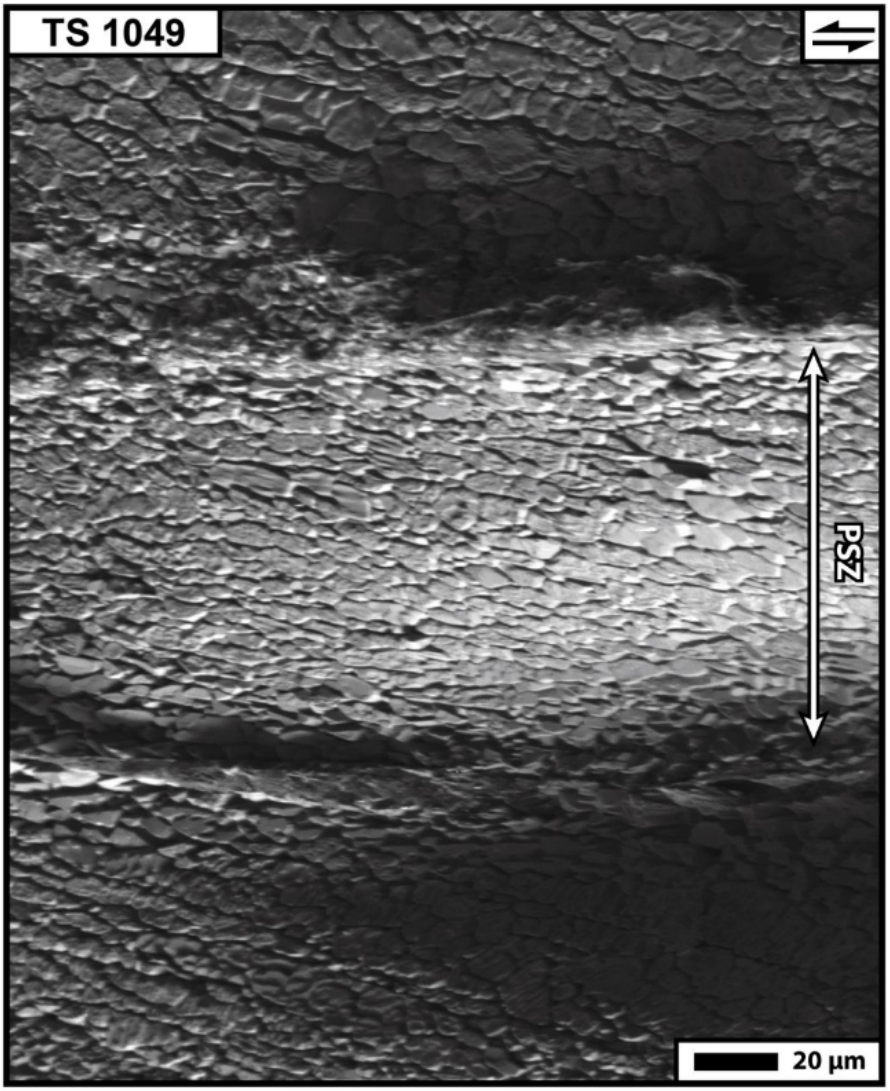

Figure 31: From (Pozzi, De Paola, Stefan Nielsen, et al. 2021)

In the previous section we have looked at evidence of crystal plasticity as a possible efficient mechanism for thermally-enhanced weakening. But temperature rise can trigger other processes that are susceptible to enhance the weakening (e.g., melt lubrication, fluid pressurization, flash weakening, or other types of flow like dislocation climb or glide, twinning).

Each thermally triggered process has a narrow temperature range at which the kinetics are exponentially accelerating and where it will become efficient. As one process is active, but temperature continues to rise under frictional work, another mechanism may kick-in that is more efficient and take over. However, change of phase triggered by the temperature rise are generally endothermal, therefore offering a thermal buffer that prevents the temperature rise.

The most efficient process will depend on the rock composition, too. Because calcite decarbonation takes place at relatively modest temperatures ($\approx 825^{o}C$), this phase transition introduces a thermal buffer that prevents reaching melting temperatures. However, when the calcite if fully decarbonated (and transformed into lime), the temperature is able to rise again **VIDEO**, until it may reach its combustion temperature (around 2500 C).

A number i of flow mechanisms could in principle be active in a latent state, however, only the most efficient one at the given temperature and grain size will be manifest:

$$\dot{\gamma}_{tot} = C_1 \, \tau^{n_1} \, e^{-\frac{H_1}{RT}} D^{m_1} + C_2 \, \tau^{n_2} \, e^{-\frac{H_2}{RT}} D^{m_2} + ... + C_i \, \tau^{n_i} \, e^{-\frac{H_i}{RT}} D^{m_i} \tag{36}$$

Minerals from rocks of different composition (e.g. silcates such granite, basalt) do not have

low decomposition temperature and are more likely to reach the melting temperature before another weakening process is triggered. In this case the flash weakening stage (localised melting of asperities) can be more or less rapidly followed by frictional melt, where a melt / clast suspension pervades the whole fault interstitial space allowing efficient melt lubrication.

Frictional melt

Frictional melt is an interesting earthquake fault process, if only because it is, to this day, the most unambiguous marker of seismic activity, and because it can be used as a gage for co-seismic frictional heating as originally proposed by Sibson 1975. Although it is unclear how pervasive it is, the solidified product of frictional melt (rapidly solidified melt: pseudotachylyte or PT) is observed on a number of exhumed natural fault outcrops.

For frictional in the presence of extrusion, one may use a modified diffusion equation with a transport term

$$\partial_t T = \kappa \partial_z^2 T + \nu \partial_z T + \frac{\delta(z)\, q}{\rho\, c}; \tag{37}$$

where ν is the migration velocity of the melting boundary. This is known as a Stefan problem, and has a simple steady-state solution in the case of $\nu = const$.

The frictional melting with extrusion dynamics can be applied to faults where most melt is extruded to lateral veins. In this case, it can be shown (S. Nielsen, Toro, T. Hirose, et al. 2008) that the normal stress dependence of friction is a powerlaw in $\sigma_n^{1/4}$, it is a form of lubrication as at high normal stress, the dependence is much weaker than the linear trend of Byerlee's friction.

- PT as a marker of seismic dynamics and directivity
- PT as a gauge for sliding friction on seismic faults
- PT as a gauge of frictional power (and slip velocity) on seismic faults

(Fig. 32)
(Fig. 33)
(Fig. 34)
(Fig. 35)
(Fig. 36)
(Fig. 38)
(Fig. 39)
(Fig. 40)
(Fig. 41)

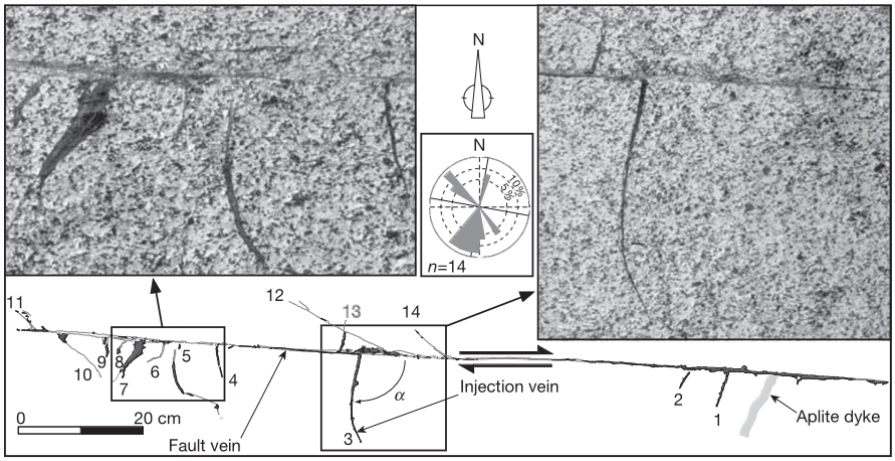
N
N
n=14
11
12
13
14
9
10
8
7
6
5
4
3
2
1
α
0
20 cm
Fault vein
Injection vein
Aplite dyke

Figure 32:

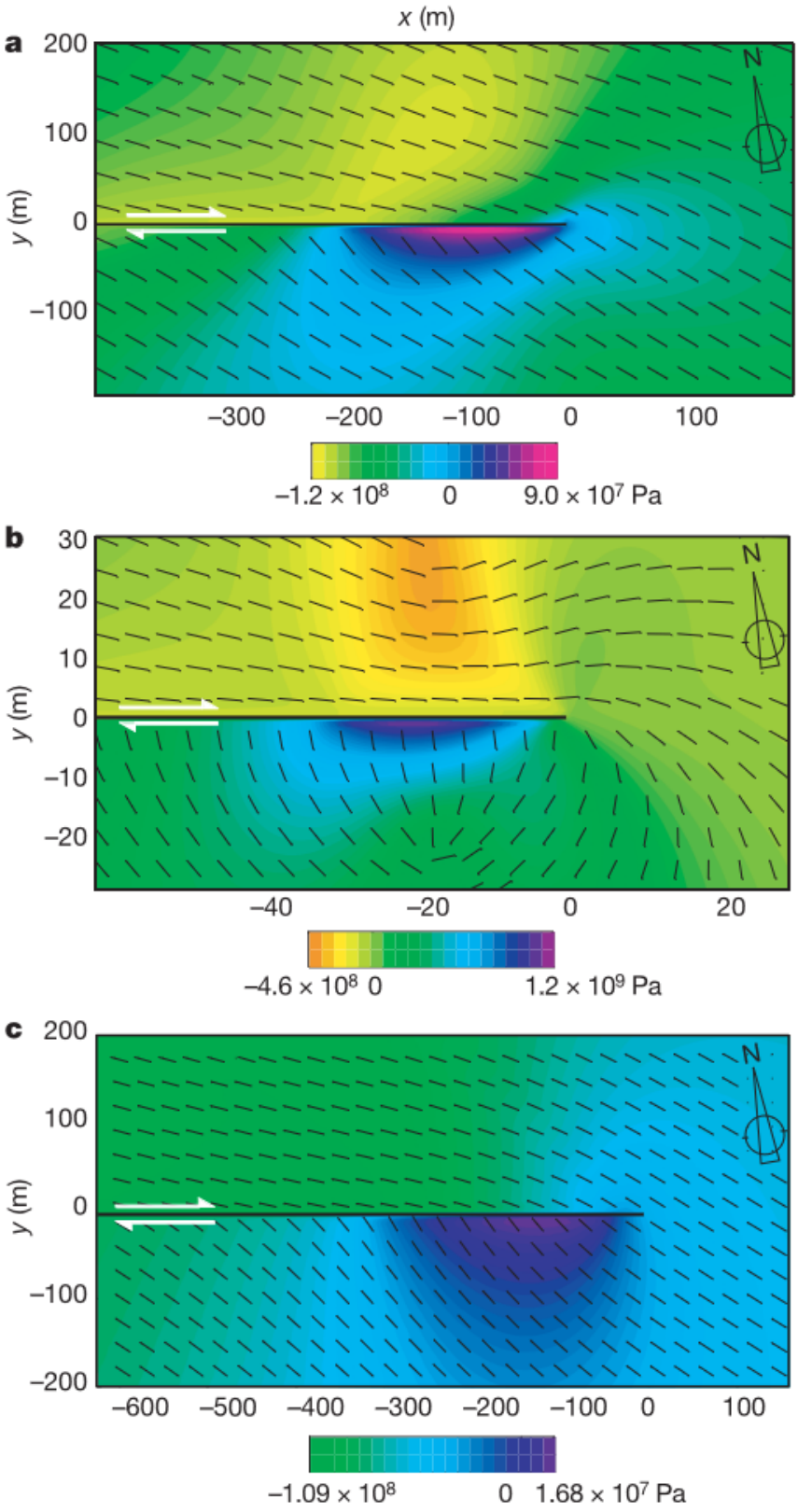

Figure 33: From (Giulio Di Toro, Stefan Nielsen, and Pennacchioni 2005)

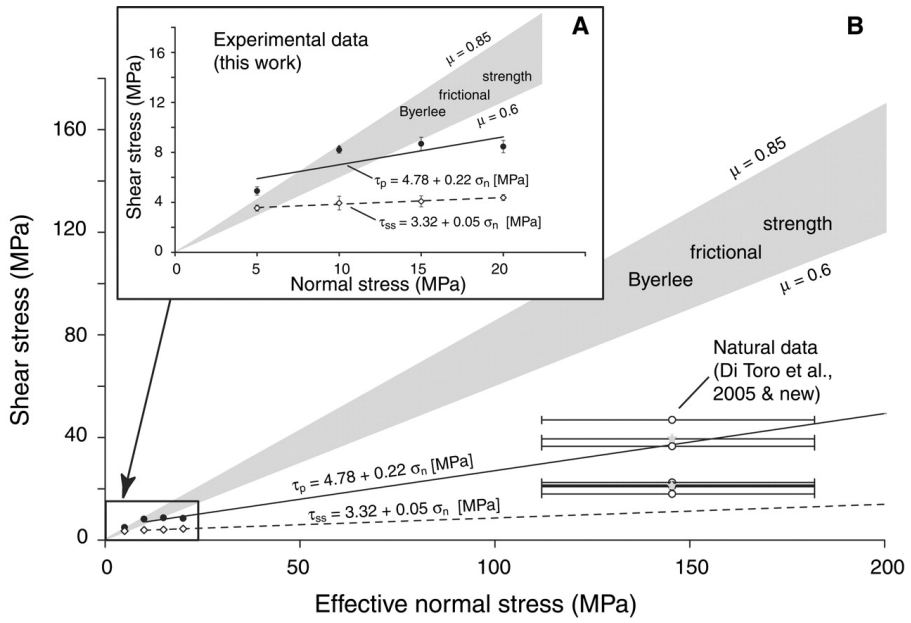

Figure 34: From (Giulio Di Toro, Takehiro Hirose, Stefan Nielsen, et al. 2006)

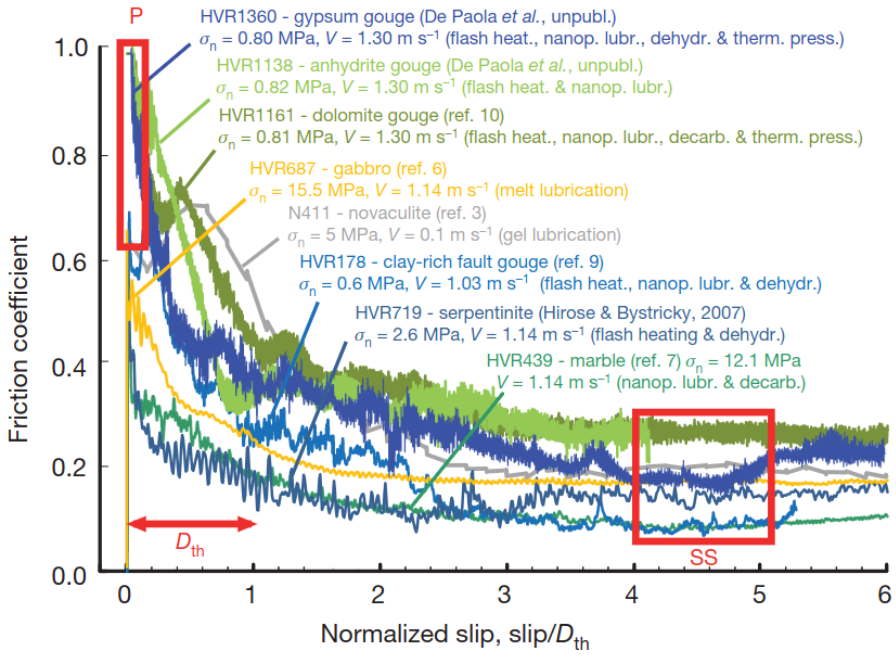

Figure 35: From (G. Di Toro, Han, T. Hirose, et al. 2011)

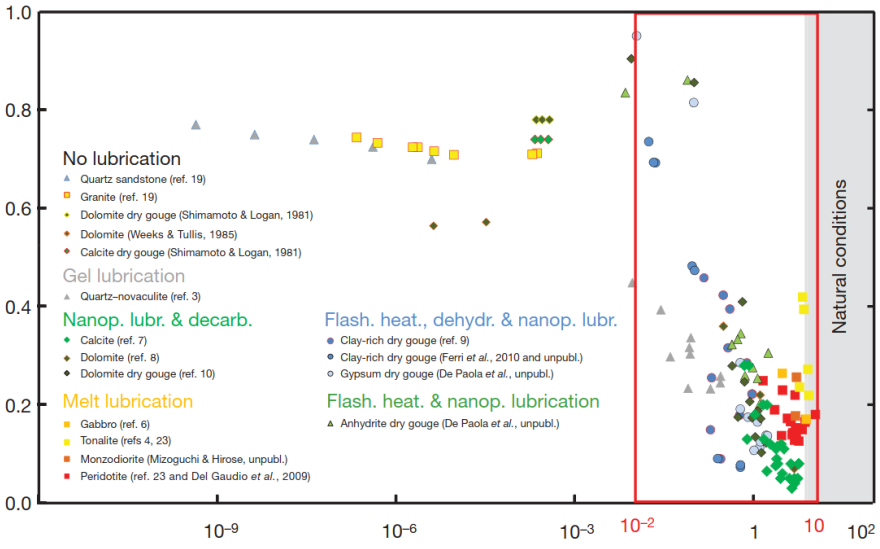

Figure 36: From (G. Di Toro, Han, T. Hirose, et al. 2011)

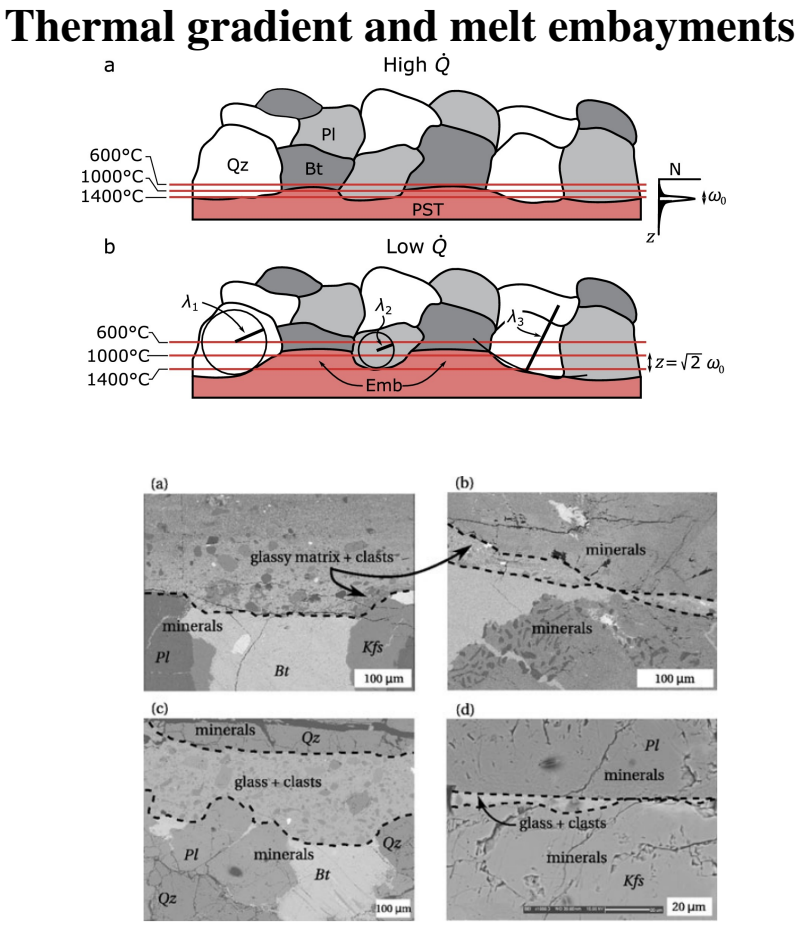

Figure 37: The thermal gradient introduces a difference in elevation (embayments) between low and high melting temperature minerals. A steeper gradient corresponding to a higher heat rate, and produces smaller embayments.

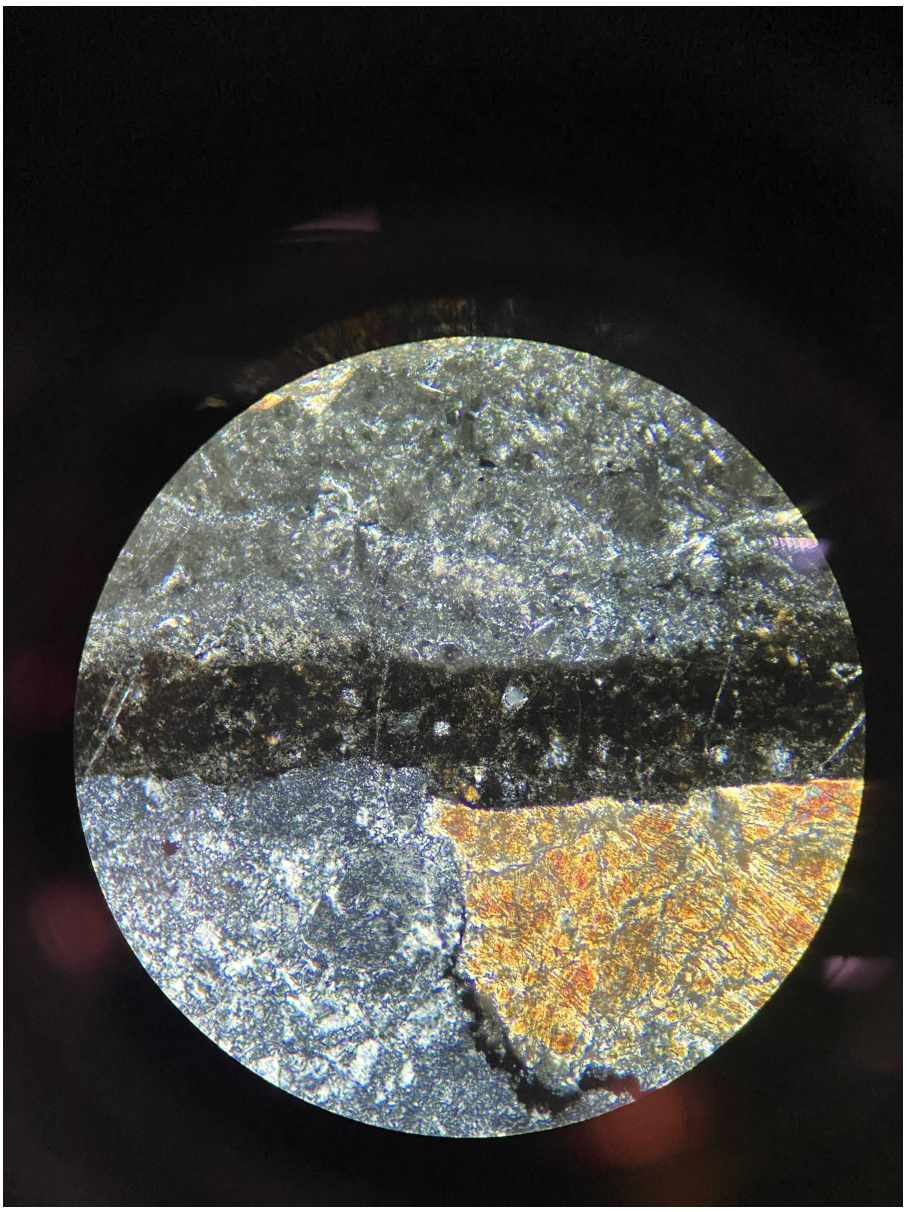

Figure 38: Peridotite (upper mantle) with PT and embayment. Field of view is ≈ 2 mm. Origin of the sample Balmuccia, Western Alps, Italy. Spinel has a lower melting temperature than Orthopyroxene by a few hundred degrees, which creates the embayment in the PT / mineral boundary on the bottom side of the fault vein.

In the field

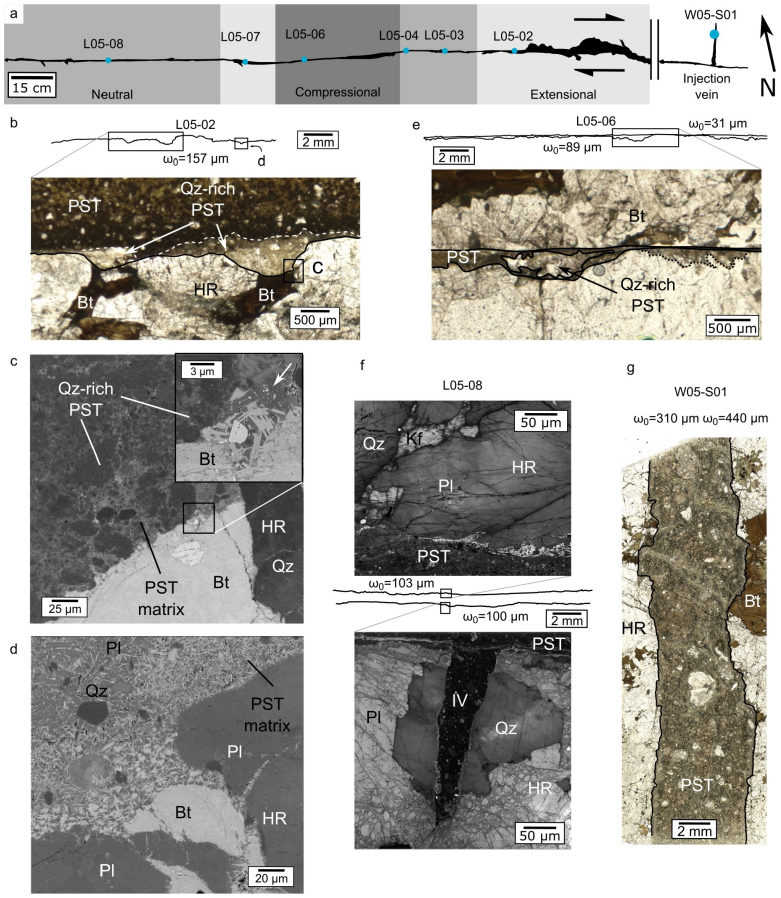

Figure 39: Fault vein and microstructures

In the Experiment

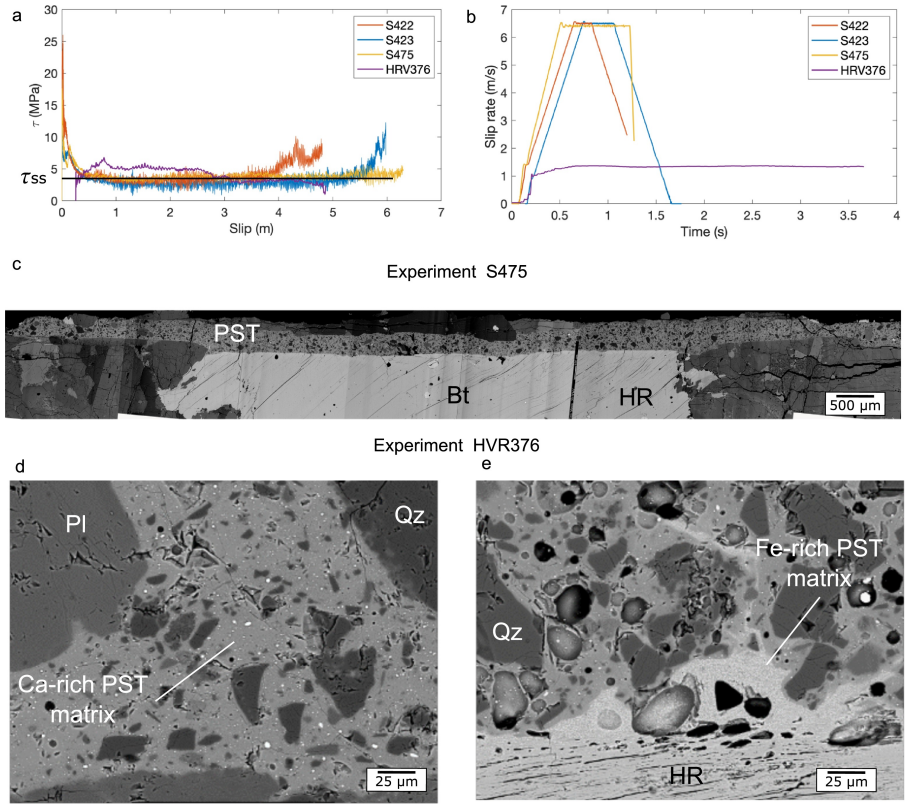

Figure 40: Experiment and PT micro-roughness. From Lazari, Castagna, S. Nielsen, et al. 2023

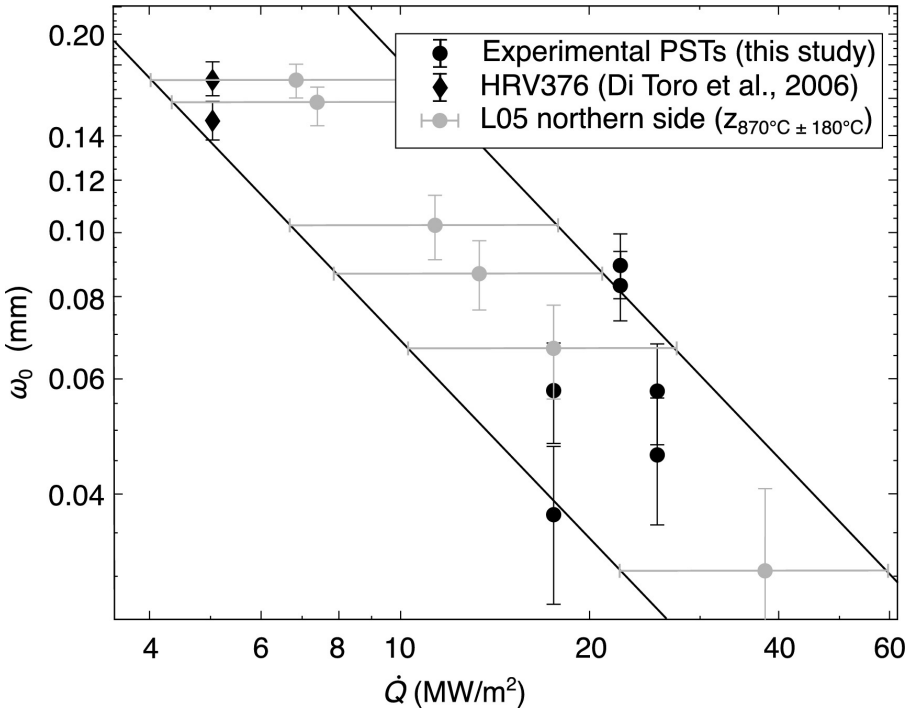

Figure 41: From(Lazari, Castagna, S. Nielsen, et al. 2023)

Exercise:

Find the steady state solution to 37 inside the solid, with $\nu = const$. Hint: use T_m (melting temperature) as a boundary condition, no heat source (it's only inside the melt), and use a moving boundary attached to the solid/melt boundary. (To check your result, see solution in S. Nielsen, Toro, T. Hirose, et al. 2008.

Fluid pressurization

- Buffering of flash weakening by fluids

Fluid pressurization is another mechanism that produces fault weakening as a consequence of frictional heating. The direct effect of pressure P_f is to relieve the effective normal stress by an amount αP where α is the Biot coefficient. α is poorly constrained and usually the limit value $\alpha = 1$ is assumed. The pressure increase is linked to the thermal expansion coefficient of the fluid (often brine or water) in a confined volume. Because friction is proportional to normal stress –save on lubricated interfaces– then the pressure results in a reduction of sliding frictional stress proportional to P_f $\tau = \mu(\sigma_n - \alpha P_f)$

However P_f is not directly proportional to T rise; indeed a change in the fault vein volume will take place in response to pressurization. In addition, the permeability of the host rock is an important parameter, and secondary fractures in the host rock will provide escape routes for the fluid, thus alleviating the pressure rise.

Recent experiments (Acosta, Passelègue, Schubnel, et al. 2018) suggest that flash heating and pressurization can compete with each other during seismic slip, and the dominant mechanism will depend on factors such as initial fluid pressure. At low (1 MPa) fluid pressure conditions or in dry conditions, flash weakening will dominate. Under higher fluid pressure (25 MPa), water's liquid-supercritical phase transition absorbs sufficient heat to buffer the temperature rise. This buffer effect is decreasing again at depths greater than a few kilometers.

(Fig. 42)

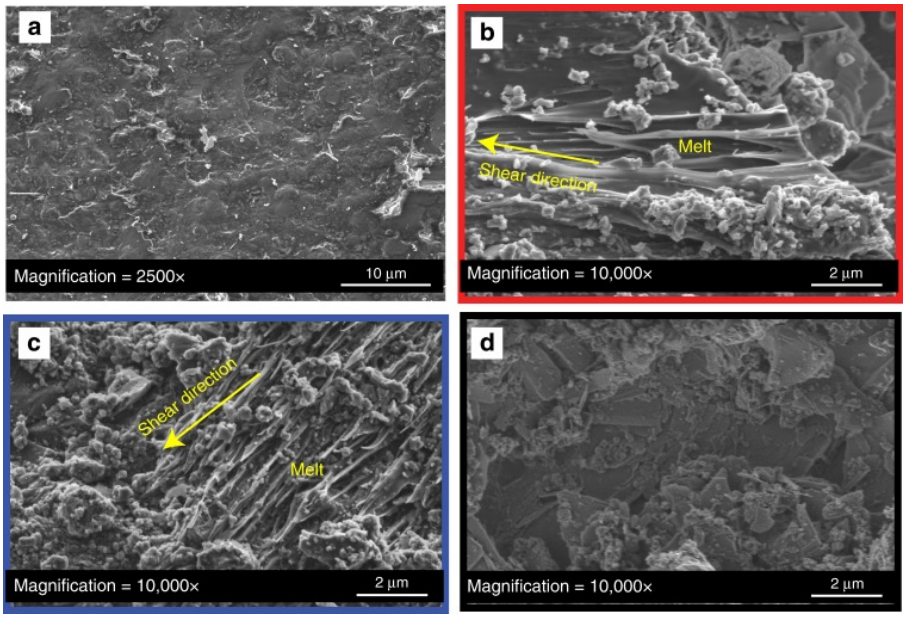

Figure 42:

The pressurization does not necessarily affect the fluid that is present in the rock from the outset, but also fluids that are the by-product of thermal decomposition. One example is the decarbonation of

dolomite that is believed to have take place in the giant landslide of Heart Mountain (T. M. Mitchell, S. A. Smith, Anders, et al. 2015). The dolomite grains adjacent to the PSZ contain vesicular rims and planar trails of vesicles typical of decarbonation. An experimental analog was produced in the laboratory as shown in **(Fig. 43)**

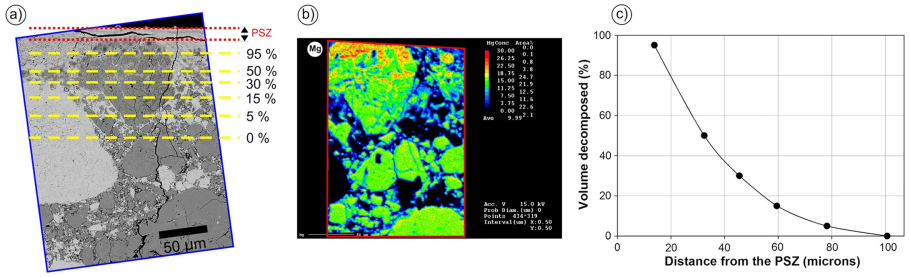

Figure 43:

Slip arrest and friction recovery

Rate-weakening and the healing effect, cracks and pulses, dynamic complexity, cf. Bruce Shaw!...

Practical projects –your choice!

1. Evaluate friction from melt volume on fossil earthquake rocks. Is it very low, and why? Is it independent of slip, and why? If there is a slip dependence, what type of function appears to fit it best (use loglog maybe)? Is there a characteristic length?

   To do this, use that shear stress times slip is work per unit fault area (N m^{-2}), and that melt volume is proportional to the amount of heat produced by frictional shear per unit fault area. You should use Table (1) and the following parameters: latent heat L=400 10^3J kg^{-1}, mass density ρ=2800 kg m^{-3} , heat capacity C_p =1200 J kg^{-1} C^{-1} , clast fraction within melt ϕ = 0.05, average melting temperature T_m =1300 C, depth = 8 km, vertical thermal gradient 25^{o}C km^{-1} . Useful equations:

$$\tau \times U = w \times E \times \rho \tag{38}$$

$$E = L(1-\phi) + C_p(T_m - T_i) \tag{39}$$

2. Compute equivalent $\mathbf{G_c}$ from friction experimental data. How does it compare to seismological estimates? Use the data from rotary sherar experiments S324, S543 and S620 in files S0620_SlipStress.csv, slistre324.csv, slistre543.csv.

3. Quantify dissipation in a distributed volume (multiple fault strands). Discuss your strategy to integrate this in the energy balance. How to integrate such a dissipation in fracture energy, or in friction, or both?

   Use the table in file *fracture-energy_data.xlsx* that reports slip measured on each of the observed sub-faults. Use the linear slip-weakening approximation of figure **(Fig. 44)** with $\tau_p = 6$ MPa, $\tau_r = 0.9$ MPa, $D_w = 0.06$m ($G_c = E_G$ is the blue area triangle).

4. Frictional heating: compute temperature, heat, and potential phase transitions at different slip rates. How early in the slip is the transition expected in real Earth conditions?

Separation	Thickness	Separation	Thickness
mm	mm	mm	mm
7.0	0.5	75.0	1.4
3.4	0.2	43.0	0.4
28.0	1.3	65.0	0.3
18.0	0.5	57.0	0.6
67.0	1.5	420.0	3.1
88.0	1.8	630.0	2.8
82.0	1.5	480.0	1.9
71.0	1.3	78.0	1.6
58.0	1.0	49.0	0.4
117.0	2.0	94.0	1.3
68.0	0.8	82.0	0.7
243.0	2.3	150.0	1.8
1290.0	7.5	310.0	1.4
910.0	3.3	59.0	0.6
22.0	0.3	275.0	1.3
24.0	1.1	685.0	2.8
12.0	0.7	35.0	0.4
55.0	1.4	43.0	0.5
31.0	0.4	41.0	0.6
26.0	0.2	76.0	0.7
80.0	1.4	120.0	0.7
25.0	0.5	46.0	0.3
18.0	0.8	11.0	0.5
65.0	0.8	1670.0	1.8

Table 1: Data measured on pseudtachylyte-bearing faults in the outer Hebrides. Separation is the apparent offset measured in the field across the fault; here we assume that separation equates to slip (i.e., that the outcrop surface was parallel to the slip direction). The thickness is an average (obtained by dividing the pseudotachylyte area visible at the surface, by the fault length). Data from (S. Nielsen, Mosca, Giberti, et al. 2010; Sibson 1975). Depth at time of seismicity: 7-9 km.

5. Compute frictional shear stress from plastic flow laws
6. Calculate rupture velocity on a simple mathematical fault, using a stress intensity K-integral
7. Calculate dynamic rupture with a prescribed friction law using a numerical modelling (finite differences, finite elements, code of Ampuero?). Compare to the K-integral.

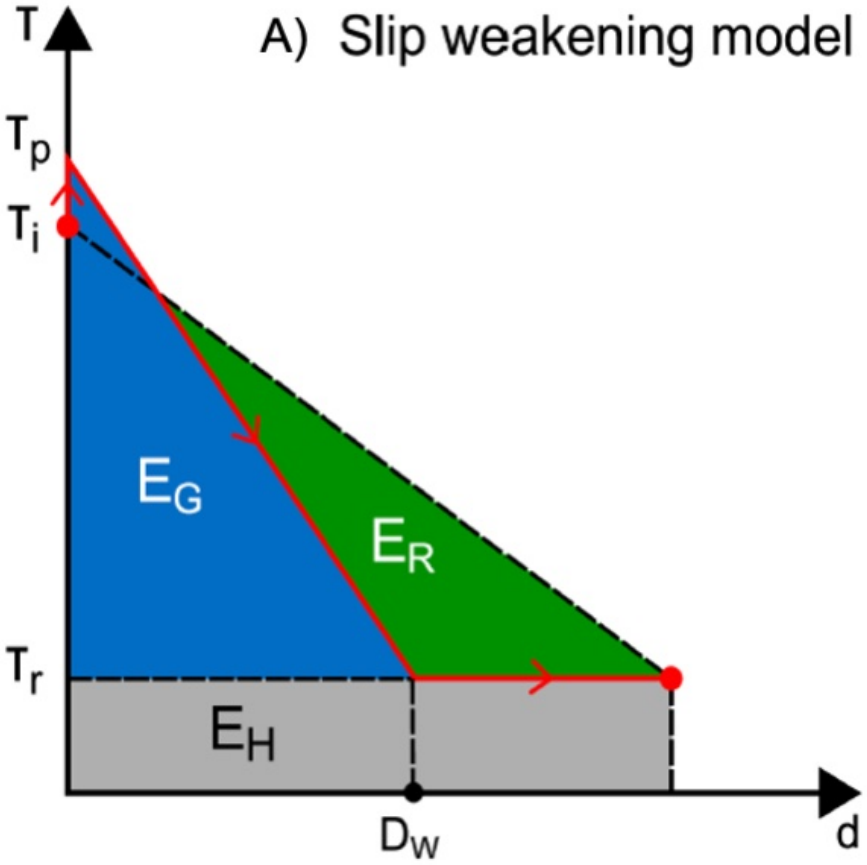

Figure 44:

Appendix I. Divergence theorem and energy

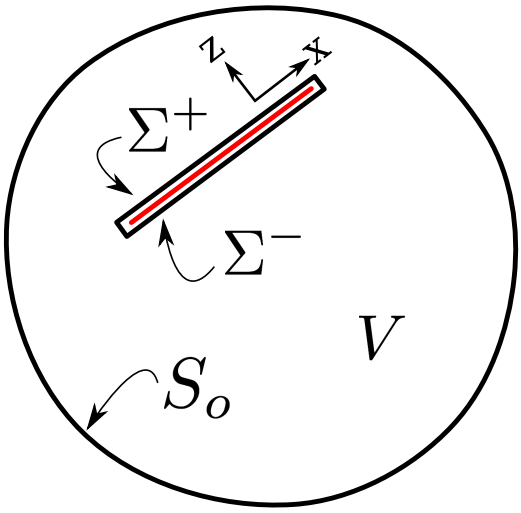

Figure 45: Schematic section of the Earth intersecting a fault surface (in red). The total Earth volume is V, S_o is the traction-free surface of the Earth, and the surface $\Sigma = \Sigma^+ + \Sigma^-$ snugly surrounds the fault. By making Σ^+ and Σ^- infinitesimally close, the volume between S and Σ can include all of V.

A full treatment of the energy change in earthquake can be found in Kostrov, Dhalen (...), which is here presented in a simplified fashion. First we state the divergence theorem. For a vector field $\mathbf{F}$ in a volume V, enclosed within a surface S:

$$\iiint_V (\nabla \cdot \mathbf{F})\, dV = \oiint_S (\mathbf{F} \cdot \mathbf{n})\, dS. \tag{40}$$

and its equivalent formulation applied to a tensor σ or σ_{ij} using Einstein notation (implicit summation on repeated indexes) for a tensor:

$$\iiint_V \partial_j \left(\sigma_{ij}\right)\, dV = \oiint_S n_j\, \sigma_{ij}\, dS. \tag{41}$$

where n_i is the i_{th} componenet of the local normal vector $\mathbf{n}$ pointing outwards from the surface S. Second, we recall the definintion of strain energy density (p.u. volume) as the product of stress and strain, namely

$$\rho_{\text{strain}} = 1/2\ \ \sigma_{ij}\, \varepsilon_{ij} \tag{42}$$

(with implicit summation over all indexes i, j). The earthquake "driving energy" E originates in the release of stored elastic strain, which is converted to in forms, including frictional dissipation, creation of new fractures and radiation of kinetic energy (waves). The difference between the stored strain energy *before* and *after* the rupture, in terms of local density, can be written as:

$$\rho_E \ \ = 1/2\ \left(\sigma^1_{ij}\varepsilon^1_{ij}\ - \sigma^0_{ij}\varepsilon^0_{ij}\right) \tag{43}$$

where the superscripts 1 and 0 refer to the final and initial conditions, respectively. then the total strain energy change E_{tot} can be obtained by integrating in the volume V surrounding the fault:

$$E_{tot} \ \ = 1/2 \iiint_V \left(\sigma^1_{ij}\varepsilon^1_{ij}\ - \sigma^0_{ij}\varepsilon^0_{ij}\ \right)\, dV \tag{44}$$

From ρ_w of eq. (43) let's try to get an expression based only on on initial stress σ^0_{ij}, stress difference $\Delta\sigma_{ij} = \sigma^1_{ij} - \sigma^0_{ij}$ and strain difference $\Delta\varepsilon_{ij} = \varepsilon^1_{ij} - \varepsilon^0_{ij}$:

$$\begin{aligned} \rho_E &= 1/2 \left(\sigma^0_{ij} + \Delta\sigma_{ij}\right) \left(\varepsilon^0_{ij} + \Delta\varepsilon_{ij}\right) - 1/2 \ \sigma^0_{ij}\varepsilon^0_{ij} \\ &= 1/2 \left(\sigma^0_{ij}\Delta\varepsilon_{ij} + \Delta\sigma_{ij}\varepsilon^0_{ij} + \Delta\sigma_{ij}\Delta\varepsilon_{ij}\right) \end{aligned} \tag{45}$$

To further simplify the expression, we can assume purely elastic strain in the volume surrounding the fault, with a constitutive law (Hooke's law) relating stress term to strain via the linear elasticsity.

Take good note here that we apply the divergence theorem only to the elastic part of the deformation. Therefore, we will need to exclude form this energy change using the divergence theorem, all volumes of rock where nonlinear or anelasic processes take place, and treat those separately. In particular, volumes within which plastic deformation or frictional dissipative processes take place will be excluded. In this specific treatment, we will assume that they take place within a volume of infinitesimal thickness –a mathematical fault surface.

For convenience we may use the elastic modules tensor c_{ijkl} such that:

$$c_{ijkl} = \lambda \ \delta_{ij}\delta_{kl} + G \left(\delta_{ik}\delta_{jl} + \delta_{il}\delta_{jk}\right) \tag{46}$$

and then write the stress-strain Hooke's law as:

$$\begin{aligned} &\sigma_{ij} = c_{ijkl} \ \varepsilon_{kl} \\ &\Delta\sigma_{ij} = c_{ijkl}\Delta\varepsilon_{kl} \\ &\varepsilon^0_{ij} = \frac{\sigma^0_{kl}}{c_{klij}} \end{aligned} \tag{47}$$

therefore

$$\begin{aligned} \rho_E &= 1/2 \left(\sigma^0_{ij} + \Delta\sigma_{ij}\right) \left(\varepsilon^0_{ij} + \Delta\varepsilon_{ij}\right) - 1/2 \ \sigma^0_{ij}\varepsilon^0_{ij} \\ &= 1/2 \left(\sigma^0_{ij}\Delta\varepsilon_{ij} + \cancel{c_{ijkl}}\Delta\varepsilon_{kl} \ \frac{\sigma^0_{kl}}{\cancel{c_{klij}}} + \Delta\sigma_{ij}\Delta\varepsilon_{ij} \right) \\ &= 1/2 \left(\sigma^0_{ij}\Delta\varepsilon_{ij} + \Delta\varepsilon_{kl} \ \sigma^0_{kl} + \Delta\sigma_{ij}\Delta\varepsilon_{ij}\right) \end{aligned} \tag{48}$$

where the symmetry property $c_{ijkl} = c_{klij}$ has been used to eliminate the elastic moduli. Because of the implicit summation all repeated indexes are dummies so we know that $\Delta\varepsilon_{kl} \ \sigma^0_{kl} = \Delta\varepsilon_{ij} \ \sigma^0_{ij}$ and therefore after replacing the $\Delta\sigma_{ij}$ we obtain:

$$\rho_E = 1/2 \ \Delta\varepsilon_{ij} \left(\sigma^0_{ij} + \sigma^1_{ij}\right) \tag{49}$$

The total energy change is otained by integrating the density on all the volume

$$E_{tot} = 1/2 \iiint_V \Delta\varepsilon_{ij} \left(\sigma^0_{ij} + \sigma^1_{ij}\right) dV \tag{50}$$

Furthermore we have that

$$\begin{aligned} \partial_i \left(\sigma_{ij} u_j\right) &= \partial_i \left(\cancel{\sigma_{ij}}\right) u_j + \sigma_{ij} \ \partial_i \left(u_j\right) \\ &= \sigma_{ij} \ \partial_i \left(u_j\right) \end{aligned} \tag{51}$$

because at equilibrium $\partial_i \left(\sigma_{ij}\right) = 0$. If u_i is the displacement of particles between before and after the rupture, by definition of the infinitesimal strain we have

$$\Delta\varepsilon_{ij} = 1/2 \left(\partial_i u_j + \partial_j u_i\right) \tag{52}$$

and because of the summation on all indexes we are allowed to write:

$$\sigma_{ij}\Delta\varepsilon_{ij} = \sigma_{ij}\partial_i u_j = \partial_i \left(\sigma_{ij} u_j\right) \tag{53}$$

Finally we can re-write the volume integral of W such that:

$$E_{tot} = 1/2 \iiint_V \partial_i \left[\left(\sigma^0_{ij} + \sigma^1_{ij} \right) \, u_j \right] dV \tag{54}$$

We may now apply the divergence theorem to write:

$$E_{tot} = 1/2 \iiint_V \partial_i \left[\left(\sigma^0_{ij} + \sigma^1_{ij} \right) \, u_j \right] dV = 1/2 \iint_S n_i \left(\sigma^0_{ij} + \sigma^1_{ij} \right) \, u_j \, dS \tag{55}$$

We may split S into two parts $S = S_o + \Sigma$ (Fig. 45). Σ is a surface snugly fitted around the fault, and S_o is the free surface of the Earth. Now because the free traction condition on the surface S_o is $\mathbf{T}(\mathbf{n}) = 0$ where $\mathbf{T}$ is traction; traction and stress are related by $T_j = \sigma_{ji} \, n_i$. Therefore the integral over S_o will vanish at any time, and we're left with

$$E_{tot} = 1/2 \iint_\Sigma n_i \left(\sigma^0_{ij} + \sigma^1_{ij} \right) \, u_j \, d\Sigma \tag{56}$$

So we have been able to show that the total energy change can be represented by a surface which can be made arbitrarily close to the fault surface, until we are for all practical purposes describing values of σ_{ij} and u_i which are effectively *on* the fault surface. To further simplify the expression, we can use a geometry where the fault normal is z, the fault is located along (x,y) plane at $z = 0$ and the slip occurs in direction x (Fig. 45). In this case the fault normal vector is $\mathbf{n} = (n_x, n_y, n_z) = (0,0,1)$, slip motion on the fault is $\mathbf{u} = (u_x, 0, 0)$ and

$$E_{tot} = 1/2 \iint_\Sigma \left(\sigma^0_{zx} + \sigma^1_{zx} \right) \, u_x \, d\Sigma \tag{57}$$

Letting Σ^- be adjacent to the "bottom" part of the fault ($z \to 0^-$) and Σ^+ be adjacent to the "top" part of the fault ($z \to 0^+$), defining slip $D = u^+_x - u^-_x$, and using traction continuity such that $\sigma^+_{xz} = \sigma^-_{xz}$ and symmetry ($\sigma_{zx} = \sigma_{xz}$) we can write

$$\begin{aligned} E_{tot} &= 1/2 \iint_{\Sigma^+} \left(\sigma^0_{xz} + \sigma^1_{xz} \right) \, u_x \, d\Sigma - 1/2 \iint_{\Sigma^-} \left(\sigma^0_{xz} + \sigma^1_{xz} \right) \, u_x \, d\Sigma \\ &= 1/2 \iint_\Sigma \left(\sigma^0_{xz} + \sigma^1_{xz} \right) D \, d\Sigma \end{aligned} \tag{58}$$

and taking $\overline{\text{average}}$ values for stress and slip on the fault, and defining $\sigma = \sigma_{xz}$ where the subscripts are implicit we can write:

$$\begin{aligned} E_{tot} &= 1/2 \iint_\Sigma \left(\sigma^0_{xz} + \sigma^1_{xz} \right) D \, d\Sigma \\ &= \frac{\overline{\sigma^0 + \sigma^1}}{2} \, \overline{D} \iint_\Sigma d\Sigma \\ E_{tot} &= \frac{\overline{\sigma^0 + \sigma^1}}{2} \overline{D} \, \Sigma \end{aligned} \tag{59}$$

Expression (59) shows that the total energy change in the volume can be calculated from the initial and final stress defined on the fault surface Σ alone. The only net work applied to the Earth-system during the earthquake is the result of the stress change on the fault surface (provided that all nonlinear processes are confined onto the surface).

References

Abercrombie, Rachel E. and James R. Rice (Aug. 2005). "Can observations of earthquake scaling constrain slip weakening?" In: *Geophysical Journal International* 162.2, pp. 406–424. DOI: 10.1111/j.1365-246x.2005.02579.x.

Acosta, M. et al. (2018). "Dynamic weakening during earthquakes controlled by fluid thermodynamics". In: *Nature Communications* 9.1. DOI: 10.1038/s41467-018-05603-9.

Aki, K and P. Richards (2002). *Quantitative Seismology, second edition*. Science University Books.

Aldrighetti, Silvia (2023). "Estimate of seismic surface energy from microstructural studies of pseudotachylyte- bearing faults". In: *TESI DI LAUREA MAGISTRALE IN GEOLOGIA AMBIENTALE E DINAMICA DELLA TERRA, Universita di Padova*.

Archard, J.F. (1959). "The temperature of rubbing surfaces". In: *Wear* 2.6, pp. 438–455. ISSN: 0043-1648. DOI: 10.1016/0043-1648(59)90159-0.

Brown, Stephen R. and Christopher H. Scholz (June 1985). "Closure of random elastic surfaces in contact". In: *Journal of Geophysical Research: Solid Earth* 90.B7, pp. 5531–5545. DOI: 10.1029/jb090ib07p05531.

Candela, Thibault et al. (Aug. 2012). "Roughness of fault surfaces over nine decades of length scales". In: *Journal of Geophysical Research: Solid Earth* 117.B8, n/a–n/a. DOI: 10.1029/2011jb009041.

Carslaw, H. S. and J. C. Jaeger (1990). *Conduction of Heat in Solids*. Oxford University Press, USA.

Cocco, Massimo et al. (2023). "Fracture Energy and Breakdown Work During Earthquakes". In: *Annual Review of Earth and Planetary Sciences* 51.1, pp. 217–252. DOI: 10.1146/annurev-earth-071822-100304.

Davies, J. H. and D. R. Davies (Feb. 2010). "Earth's surface heat flux". English. In: *Solid Earth* 1.1. Publisher: Copernicus GmbH, pp. 5–24. ISSN: 1869-9510. DOI: 10.5194/se-1-5-2010. (Visited on 09/27/2023).

Di Toro, G. et al. (Mar. 2011). "Fault lubrication during earthquakes". In: *Nature* 471.7339, pp. 494–498. DOI: 10.1038/nature09838.

Di Toro, Giulio, Stefan Nielsen, and Giorgio Pennacchioni (Aug. 2005). "Earthquake rupture dynamics frozen in exhumed ancient faults". In: *Nature* 436.7053, pp. 1009–1012. DOI: 10.1038/nature03910.

Di Toro, Giulio et al. (Feb. 2006). "Natural and Experimental Evidence of Melt Lubrication of Faults During Earthquakes". In: *Science* 311.5761, pp. 647–649. DOI: 10.1126/science.1121012.

Dieterich, James H. and Brian D. Kilgore (May 1996). "Imaging surface contacts: power law contact distributions and contact stresses in quartz, calcite, glass and acrylic plastic". In: *Tectonophysics* 256.1-4, pp. 219–239. DOI: 10.1016/0040-1951(95)00165-4.

Fossum, A. F. and L. B. Freund (Aug. 1975). "Nonuniformly moving shear crack model of a shallow focus earthquake mechanism". In: *Journal of Geophysical Research* 80.23, pp. 3343–3347. DOI: 10.1029/jb080i023p03343.

Goldsby, D. L. and T. E. Tullis (Oct. 2011). "Flash Heating Leads to Low Frictional Strength of Crustal Rocks at Earthquake Slip Rates". In: *Science* 334.6053, pp. 216–218. ISSN: 1095-9203. DOI: 10.1126/science.1207902.

Greenwood, J. A. and J. B. P. Williamson (1966). "Contact of nominally flat surfaces". In: *Proceedings of the Royal Society of London. Series A, Mathematical and Physical Sciences* 295.1442, pp. 300–319.

Kanamori, Hiroo and Luis Rivera (2006). "Energy partitioning during an earthquake". In: *Earthquakes: Radiated Energy and the Physics of Faulting*. American Geophysical Union, pp. 3–13. DOI: 10.1029/170gm03.

Lazari, F. et al. (2023). "Frictional power dissipation in a seismic ancient fault". In: *Earth and Planetary Science Letters* 607, p. 118057. DOI: 10.1016/j.epsl.2023.118057.

Madariaga, Raul (May 2007). "Slippery When Hot". In: *Science* 316.5826, pp. 842–843. DOI: 10.1126/science.1142332.

Mitchell, T.M. and D.R. Faulkner (Aug. 2009). "The nature and origin of off-fault damage surrounding strike-slip fault zones with a wide range of displacements: A field study from the Atacama fault system, northern Chile". In: *Journal of Structural Geology* 31.8, pp. 802–816. DOI: 10.1016/j.jsg.2009.05.002.

Mitchell, Thomas M. et al. (Feb. 2015). "Catastrophic emplacement of giant landslides aided by thermal decomposition: Heart Mountain, Wyoming". In: *Earth and Planetary Science Letters* 411, pp. 199–207. DOI: 10.1016/j.epsl.2014.10.051.

Nielsen, S., G. di Toro, and W. A. Griffith (2010). "Friction and roughness of a melting rock surface". In: *Geophysical Journal International*. DOI: 10.1111/j.1365-246x.2010.04607.x.

Nielsen, S., E. Spagnuolo, M. Violay, and G. Di Toro (2021). "Thermal Weakening Friction During Seismic Slip: Experiments and Models With Heat Sources and Sinks". In: *Journal of Geophysical Research: Solid Earth* 126.5. DOI: 10.1029/2020jb020652.

Nielsen, S., E. Spagnuolo, M. Violay, S. Smith, et al. (Mar. 2016). "G: Fracture energy, friction and dissipation in earthquakes". In: *Journal of Seismology* 20.4, pp. 1187–1205. DOI: 10.1007/s10950-016-9560-1.

Nielsen, S. et al. (Jan. 2008). "Frictional melt and seismic slip". In: *Journal of Geophysical Research: Solid Earth* 113.B1. DOI: 10.1029/2007jb005122.

Nielsen, S. et al. (2010). "On the transient behavior of frictional melt during seismic slip". In: *Journal of Geophysical Research: Solid Earth* 115.B10. DOI: https://doi.org/10.1029/2009JB007020.

Nielsen, S. et al. (2016). "Scaling in natural and laboratory earthquakes". In: *Geophysical Research Letters* 43.4. 2015GL067490, pp. 1504–1510. ISSN: 1944-8007. DOI: 10.1002/2015GL067490.

Pacheco, Javier F. and Lynn R. Sykes (June 1992). "Seismic moment catalog of large shallow earthquakes, 1900 to 1989". In: *Bulletin of the Seismological Society of America* 82.3, pp. 1306–1349. ISSN: 0037-1106. DOI: 10.1785/BSSA0820031306.

Persson, B. (2000). *Sliding Friction, Physical Principles and Applications*. Springer-Verlag, New York.

Pozzi, Giacomo et al. (2021). "Coseismic fault lubrication by viscous deformation". In: *Nature Geoscience* 14, pp. 437–442. ISSN: 1752-0894. DOI: 10.1038/s41561-021-00747-8.

Reches, Zeev, Xiaofeng Chen, and Brett Carpenter (2019). "Asperity failure control of stick-slip along brittle faults". In: *ESSOAR*. DOI: 10.1002/essoar.10501044.1.

Rice, J. R. (2006). "Heating and weakening of faults during earthquake slip". In: *J. Geophys. Res.* 111, B05311. DOI: 10.1029/2005JB004006.

Sibson, Richard H. (1975). "Generation of Pseudotachylyte by Ancient Seismic Faulting". In: *Geophysical Journal of the Royal Astronomical Society* 43.3, pp. 775–794. DOI: https://doi.org/10.1111/j.1365-246X.1975.tb06195.x.

Spagnuolo, E. et al. (Apr. 2016). "An empirically based steady state friction law and implications for fault stability". In: *Geophysical Research Letters* 43.7, pp. 3263–3271. DOI: 10.1002/2016gl067881.

Stern, Robert J. (2002). "Subduction Zones". en. In: *Reviews of Geophysics* 40.4, pp. 3–1–3–38. ISSN: 1944-9208. DOI: 10.1029/2001RG000108.

Violay, M. et al. (2015). "Thermo-mechanical pressurization of experimental faults in cohesive rocks during seismic slip". In: *Earth Planet. Sci. Lett.* 429, pp. 1–10. ISSN: 0012-821X. DOI: 10.1016/j.epsl.2015.07.054.

Xu, Shiqing et al. (Sept. 2014). "Dynamic Ruptures on a Frictional Interface with Off-Fault Brittle Damage: Feedback Mechanisms and Effects on Slip and Near-Fault Motion". In: *Pure and Applied Geophysics* 172.5, pp. 1243–1267. DOI: 10.1007/s00024-014-0923-7.